



Cite this: *Mater. Horiz.*, 2023, 10, 1185

## Surface engineering of colloidal nanoparticles

Xinxin Jing,<sup>†[a](#)</sup> Yueyue Zhang,<sup>†[a](#)</sup> Min Li,<sup>a</sup> Xiaolei Zuo,<sup>ID ab</sup> Chunhai Fan <sup>ID \*[b](#)</sup> and Junhua Zheng<sup>\*[a](#)</sup>

Synthesis of engineered colloidal nanoparticles (NPs) with delicate surface characteristics leads to well-defined physicochemical properties and contributes to multifunctional applications. Surface engineering of colloidal NPs can improve their stability in diverse solvents by inhibiting the interparticle attractive forces, thus providing a prerequisite for further particle manipulation, fabrication of the following materials and biological applications. During the last decades, surface engineering methods for colloidal NPs have been well-developed by numerous researchers. However, accurate control of surface properties is still an important topic. The emerging DNA/protein nanotechnology offers additional possibility of surface modification of NPs and programmable particle self-assembly. Here, we first briefly review the recent progress in surface engineering of colloidal NPs, focusing on the improved stability by grafting suitable small molecules, polymers or biological macromolecules. We then present the practical strategies for nucleic acid surface encoding of NPs and subsequent programmable assembly. Various exciting applications of these unique materials are summarized with a specific focus on the cellular uptake, bio-toxicity, imaging and diagnosis of colloidal NPs *in vivo*. With the growing interest in colloidal NPs in nano-biological research, we expect that this review can play an instructive role in engineering the surface properties for desired applications.

Received 12th December 2022,  
Accepted 16th January 2023

DOI: 10.1039/d2mh01512a

rsc.li/materials-horizons

<sup>a</sup> Department of Urology, Institute of Molecular Medicine, Shanghai Key Laboratory for Nucleic Acid Chemistry and Nanomedicine, Renji Hospital, School of Medicine, Shanghai Jiao Tong University, Shanghai, 200127, China.

E-mail: zhengjh0471@sina.com

<sup>b</sup> School of Chemistry and Chemical Engineering, Zhangjiang Institute for Advanced Study, Frontiers Science Center for Transformative Molecules and National Center for Translational Medicine, Shanghai Jiao Tong University, Shanghai, 200240, China. E-mail: fanchunhai@sjtu.edu.cn

† X. X. Jing and Y. Y. Zhang contributed equally to this work



**Xinxin Jing**

Xinxin Jing received his PhD degree (2014–2019) from the Shanghai Institute of Applied Physics (SINAP), Chinese Academy of Sciences. He worked as a postdoctoral researcher at the Institute of Molecular Medicine, School of Medicine, Shanghai Jiao Tong University (2019–2022), and 2nd Physics Institute, University of Stuttgart (2022–present). His research interests are mainly focused on DNA nanotechnology and biomimetic mineralization.



**Yueyue Zhang**

## 1 Introduction

Colloidal nanoparticles (NPs) whose size, shape, composition, and surface characteristics can be precisely manipulated hold great promise for both scientific research and practical applications (pharmacy, ceramics and catalysts). Due to their inherent properties, a variety of colloidal NPs, such as nonmetallic oxide NPs like solid SiO<sub>2</sub><sup>1</sup> or mesoporous SiO<sub>2</sub>,<sup>2</sup> metallic oxide NPs like Fe<sub>3</sub>O<sub>4</sub>,<sup>3</sup> metallic NPs like AuNPs,<sup>4</sup> carbon-based nanomaterials like carbon nanotubes (CNTs)<sup>5</sup> and quantum dots (QDs),<sup>6</sup> have

Yueyue Zhang received her PhD degree (2017–2020) from the Shanghai Institute of Applied Physics (SINAP), Chinese Academy of Sciences. She worked as a postdoctoral researcher (2020–2022) and then as an assistant professor (2022–Present) at the Institute of Molecular Medicine, School of Medicine, Shanghai Jiao Tong University. Her research interests are mainly focused on DNA nanotechnology, nucleic acid information materials and interface regulation.

## Review

## Materials Horizons

provided unprecedented advantages. For instance, the high specific surface area and large pore volume of mesoporous  $\text{SiO}_2$  significantly enhance their nanodrug loading capacity.<sup>2</sup> Additionally,  $\text{Fe}_3\text{O}_4$  magnetite nanocrystals (MNCs), which have been dispersed in a hydrophobic solvent, have numerous applications in magnetic resonance imaging,<sup>7</sup> magnetic separation,<sup>8</sup> energy storage,<sup>9</sup> and catalysis.<sup>10</sup> Moreover, AuNPs exhibit strong localized surface plasmons that profit from the ability to manipulate light, thereby providing a potent approach for the detection of cancer and photothermal therapy.<sup>11</sup> CNTs, unlike conventional spherical NPs, are hollow, cylinder-shaped carbon materials with a single-layer carbon atom wall that measures  $\sim 1$  nm in diameter and several micrometers in length.<sup>5</sup> Due to their structural characteristics and interfacial properties, CNTs have numerous potential applications, including transistors, logic gates, sensors, scanning probes, information storage, catalysis, and nanodevices.<sup>12–17</sup>

Even though colloidal NPs with excellent properties have made great strides in recent decades, inherent limitations continue to affect the stability of colloidal NPs in solutions. Correspondingly, the thermodynamic instability of colloidal



Min Li

*Min Li received her PhD degree (2013–2018) from the Shanghai Institute of Applied Physics (SINAP), Chinese Academy of Sciences. She worked as a postdoctoral researcher (2018–2020) and then as an associate professor (2020–Present) at the Institute of Molecular Medicine, School of Medicine, Shanghai Jiao Tong University. Her research interests are mainly focused on DNA nanotechnology, electrochemical biosensing, and liquid biopsy based on DNA nanostructures.*

nanoparticles leads to their aggregation reducing their high surface energy. In general, the stability of colloidal NPs is determined from the balance between attractive force and repulsive force, with the former originating from the intermolecular van der Waals (vdW) force and the latter originating from the overlap of electrical double layers (EDL) or steric hindrance. However, differences in surface functional groups and dispersing media complicate the interactions between colloidal NPs.  $\text{SiO}_2$  NPs, for instance, are typically synthesized using the traditional sol-gel process<sup>1</sup> and disperse in ethanol or water. As a result of the negative charge of silanol at neutral pH, EDL layers form on the surface of  $\text{SiO}_2$  NPs, preventing their aggregation.  $\text{SiO}_2$  NPs have a high tendency to aggregate; however, due to the polymerization activity of silanol on their surface. Thus, controlling the synthesis of  $\text{SiO}_2$  NPs or the growth of silica layers on various templates remains a formidable challenge. In contrast, the hydrophobic oleic acid molecules on the surface of synthesized  $\text{Fe}_3\text{O}_4$  MNCs stabilize them in nonpolar solvents but render them unstable in polar solvents. Moreover, unlike conventional NPs synthesized in polar/nonpolar solvent, CNTs have low stability in the majority of solvents due to the high



Xiaolei Zuo

*Xiaolei Zuo received his PhD degree from Shanghai Institute of Applied Physics, Chinese Academy of Sciences (2008). He was a postdoctoral fellow at the University of California, Santa Barbara, USA (2008–2010), and at Los Alamos National Laboratory, USA (2010–2012). Now he is a professor at the Institute of Molecular Medicine, Renji Hospital, School of Medicine, Shanghai Jiao Tong University. His research interests focus on electrochemical biosensors, framework nucleic acid, and DNA data storage.*



Chunhai Fan

*Chunhai Fan obtained his BS and PhD from the Department of Biochemistry at Nanjing University in 1996 and 2000. After his postdoctoral research at the University of California, Santa Barbara (2001–2003), he joined the faculty at SINAP, CAS (2004–2018). He is now a chair professor of the School of Chemistry and Chemical Engineering, Shanghai Jiao Tong University, China. His research interests include DNA framework-based biosensing, imaging, and biocomputing.*



Junhua Zheng

*Junhua Zheng obtained his MD degree (1992–1997) from Second Military Medical University. He worked in the Department of Urology in Shanghai Changzheng Hospital (1997–2006), Shanghai Tenth People's Hospital (2007–2017) and Shanghai General Hospital (2017–2021). Currently he is the party secretary of Renji Hospital, Shanghai Jiao Tong University School of Medicine. His research interests include clinical diagnosis, treatment and translational research in kidney cancer.*

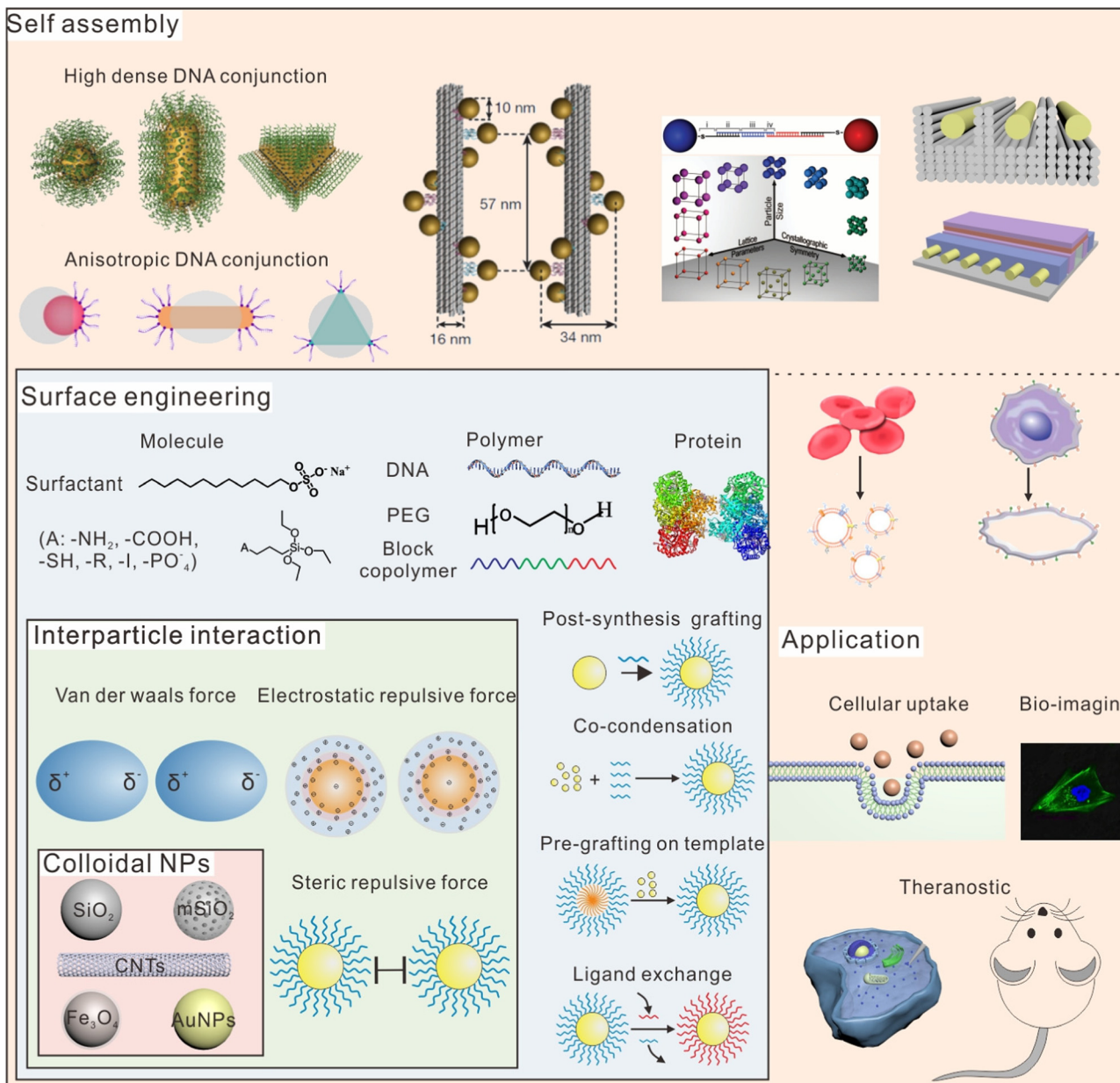


Fig. 1 Schematic illustration of the surface engineering of colloidal NPs. Reprinted with permission from ref. 93. Copyright 2012 American Chemical Society. Reprinted with permission from ref. 103. Copyright 2018 Springer Nature. Reprinted with permission from ref. 113. Copyright 2012 Springer Nature. Reprinted with permission from ref. 120. Copyright 2011 The American Association for the Advancement of Science. Reprinted with permission from ref. 132. Copyright 2020 The American Association for the Advancement of Science. Reprinted with permission from ref. 133. Copyright 2020 The American Association for the Advancement of Science. Reprinted with permission from ref. 146. Copyright 2011 National Academy of Sciences. Reprinted with permission from ref. 153. Copyright 2014 American Chemical Society. Reprinted with permission from ref. 183. Copyright 2020 John Wiley and Sons.

vDW force between adjacent CNTs. Therefore, stability has become one of the greatest challenges for colloidal NPs in application and practice. Future advancements are required to optimize both theories and methods for enhancing the environmental stability of colloidal NPs (solvent, pH, ion strength and temperature). Moreover, the ability to obtain stable colloids is not only of structural significance, but also a requirement for exploiting their inherent properties in various fields.

Surface engineering techniques such as modifying surface charge,<sup>18</sup> roughness<sup>19</sup> and hydrophilicity/hydrophobicity,<sup>20</sup> as

well as grafting biological molecules<sup>21</sup> and coating materials,<sup>22</sup> allow us to obtain NPs with excellent performance in fields like bioimaging,<sup>23</sup> catalysis,<sup>24</sup> sensing, and biological theranostics (Fig. 1).<sup>25</sup> Correspondingly, small molecules, polymers, and proteins have been used to modify the surface properties of colloidal NPs using a variety of strategies over the past few decades in order to increase stability, reverse surface charge, control self-assembly, and enhance cellular uptake. Emerging technologies (*e.g.*, DNA nanotechnology, DNA-encoded NPs assembly, and biomaterialization) facilitate the complexity

and designability of surface engineering, demonstrate great potential for programmable self-assembly, and enhance the physiological behavior of colloidal NPs. In this review, we aim to discuss three aspects of surface engineering of colloidal NPs. These include (1) stability of colloidal NPs with different surface properties in different solvents; (2) self-assembly of colloidal NPs that can be driven by surface properties; and (3) the influence of surface properties on the physiological behavior of colloidal NPs *in vivo*, including cellular uptake and cytotoxicity. Furthermore, special attention will be paid to the theoretical analysis and experimental discussion of the relationship between the aggregation behavior and surface properties. Finally, we discuss the new frontiers and challenges in the surface engineering of colloidal NPs.

## 2 Surface engineering of colloidal NPs

### 2.1 Theoretical analysis of the aggregation behavior of colloidal NPs

Stability of colloidal NPs is typically determined from the equilibrium between intermolecular vdW attractive forces<sup>26</sup> and the repulsive forces from EDL<sup>27</sup> or steric hindrance (Fig. 2a).<sup>28</sup> In aqueous environments, NPs usually carry surface charge due to the ionization of surface groups. This charge can be balanced by the formation of a cloud of counterions composed of stern layers and diffuse layers (EDL) around the NPs (Fig. 2a, left). Additionally, in the stern layer, approximately 1–2 molecules adsorb on the surface of NPs to form a stern

plane, which comprises the solvation shell boundary. The potential difference between the stern plane and the solution body is termed the electro-kinetic potential ( $\zeta$  potentials), which can be experimentally determined by dynamic light scattering (DLS), and is commonly used to access the stability of NPs in aqueous solution.<sup>29</sup> In addition,  $\zeta$  potentials are strongly correlated with surface charge values and EDL thickness, which are influenced by pH and ion concentrations. For example, the surface charge of colloidal NPs with amphoteric surfaces, such as  $\text{SiO}_2$ , is largely dependent on the pH of the solution. Correspondingly, at pH values close to the isoelectric point, the surface charge tends to be zero, and the resulting thin EDL promotes aggregation. High ion concentrations can also result in the compression of the EDL, which reduces electrostatic repulsive force and destabilizes colloidal systems.<sup>30</sup> The state of a colloidal system was determined using the Derjaguin-Landau-Verwey-Overbeek (DLVO) theory, which is a classical theoretical approach.<sup>31</sup> The DLVO theory predicts stability using the superposition of attractive vdW and electrostatic repulsive forces. As Brownian motion brings colloidal NPs closer, repulsive forces increase because of the overlap of EDLs surrounding the NPs, resulting in a rise in potential energy. However, as the inter-particle distance further decreases, the potential energy may rapidly decrease due to the increased short-range vdW attractive forces, with the magnitude inversely proportional to the sixth order of molecular distance. In general, NPs with high surface ionization can form thick EDLs, resulting in a high potential energy barrier that prevents approaching particles. Nevertheless, despite the fact that  $\text{SiO}_2$

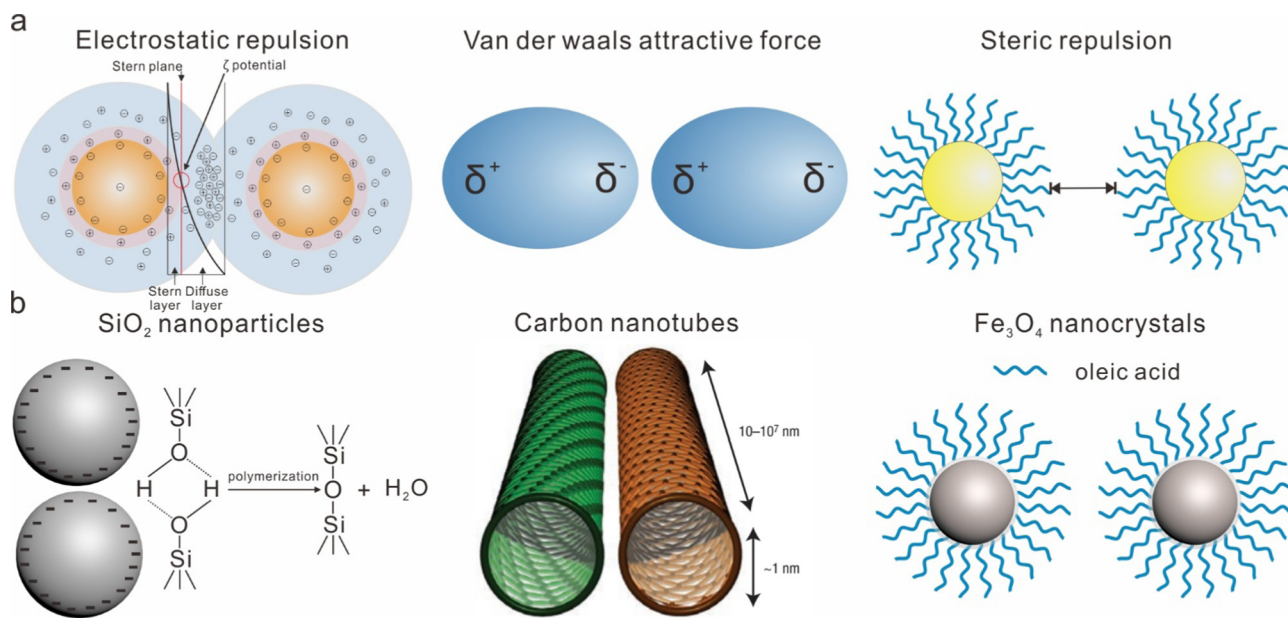


**Fig. 2** Inter-particle interaction of various colloidal NPs. (a) Three representative inter-particle interactions: electrostatic repulsion from increased EDL thickness, attractive force of vdW and steric repulsion from the attached long-chain polymers. (b) Examples for the aggregation of NPs based on three typical inter-particle interactions. For  $\text{SiO}_2$  NPs, the inter-particle interactions are complicated. Despite having surface electrostatic repulsion, they can still stick together during and after the synthetic process via polymerization. Carbon nanotubes with  $\sim 1$  nm diameter will aggregate severely in solution due to the strong vdW interactions. However,  $\text{Fe}_3\text{O}_4$  MNCs which contain capped oleic acid molecules in nonpolar solvents can introduce steric repulsion and thus maintain their stability. Reprinted with permission from ref. 5. Copyright 2016 Springer Nature.

NPs have a high  $\zeta$  potential value ( $\sim 40$  mV), they still tend to adhere and produce covalent linkage (Si–O–Si) through the chemical polymerization process (Fig. 2b, left).<sup>1</sup> In order to improve the stability of SiO<sub>2</sub> NPs, it is necessary to introduce suitable surface molecular groups to the polymerization process.

As compared to surface-charged particles, the stability of colloidal NPs without surface ionization, such as CNTs, is typically inferior. Due to the absence of electrostatic repulsive force, the highly attractive vdW forces cause a severe aggregation of CNTs in most solutions (Fig. 2a and b, middle).<sup>5,26</sup> In this regard, surface modification utilizing highly ionized molecules or polymers has been demonstrated to be a feasible and effective method for introducing repulsive forces. Additionally, steric stabilization provides a potent tool for improving the dispersion state of colloidal NPs by preventing the formation of attractive vdW interactions between particles (Fig. 2a, right). The magnitude of steric repulsive forces depends on the density and chain length of macromolecules grafted onto the surface of colloidal NPs. For example, for typical solution-phase high-temperature decomposition synthesis of monodisperse Fe<sub>3</sub>O<sub>4</sub> MNCs, a non-polar solvent is required such as benzyl ether and a ligand with a long-chain alkane such as oleic acid (Fig. 2b, right).<sup>32</sup> However, Fe<sub>3</sub>O<sub>4</sub> MNCs modified with hydrophobic molecules aggregate easily after transferring into aqueous solution, limiting the manipulation of Fe<sub>3</sub>O<sub>4</sub> MNCs and future applications. By exchanging ligands with charged macromolecules, the combination of electrostatic repulsion and steric hindrance could improve the stability of Fe<sub>3</sub>O<sub>4</sub> MNCs in aqueous solution.

As evident from the above discussion, regulating inter-particle interactions is a viable approach for obtaining colloids with a uniform distribution. In fact, chemists have developed a variety of sophisticated techniques for controlling the complex interactions and subsequent aggregation behavior of colloidal particles. These strategies pave the way for the development of numerous fascinating materials by using surface modified colloidal NPs as a building block for superstructures, or as a nanoscale drug delivery system. Relying on the exquisite surface engineering, one can, therefore, anticipate a substantial increase in structural complexity and potential applications.

## 2.2 Surface engineering of SiO<sub>2</sub> NPs for colloidal stability

Among numerous colloidal NPs, SiO<sub>2</sub> NPs play a crucial role due to their unique characteristics, which include high chemical stability, tunable pore size, excellent biocompatibility, and simple, scalable synthesis.<sup>33–35</sup> In recent decades, scientists' research interest in SiO<sub>2</sub> has risen dramatically. The primary focus of research is the engineering of particle size, shape, porosity, and various particle forms (such as solid SiO<sub>2</sub>,<sup>1</sup> mesoporous SiO<sub>2</sub>,<sup>2</sup> hollow or core–shell SiO<sub>2</sub><sup>36</sup> and caged SiO<sub>2</sub><sup>37</sup>). Additionally, the facile controllability of surface properties of SiO<sub>2</sub> NPs enables researchers to create complex composites and customized applications. Polyethylene glycol (PEG), polyethylene oxide (PEO), amines, alkyl, carboxyl, and thiol have been utilized to graft onto the surface of SiO<sub>2</sub> NPs. In this section, we will discuss three methods for modifying the surface properties of SiO<sub>2</sub>

nanoparticles, post-synthesis grafting, pre-grafting on a designed template and co-condensation, as well as give a comparative analysis of the effect of various molecular groups on the stability of SiO<sub>2</sub>.

**Post-synthesis grafting.** When diverse molecules or polymers are successfully grafted onto the synthesized SiO<sub>2</sub> NPs, desirable surface properties can be generated. PEG and PEO are the most commonly used polymers grafted on SiO<sub>2</sub> NPs due to their high solubility and thick solvation layer, which can theoretically increase the electrostatic repulsive force and steric hindrance. Bridger and Vincent reported the grafting of PEO onto the SiO<sub>2</sub> surface forty years ago.<sup>38</sup> They prepared isocyanate-capped PEO and then mixed with (3-aminopropyl)triethoxysilane to obtain triethoxysilane-terminated PEO, which was added at the late stage of the Stöber synthesis. These PEO-modified SiO<sub>2</sub> NPs were more stable than unmodified SiO<sub>2</sub> NPs; however, aggregation was still observed and free PEO was detected in solution after approximately one month of storage in aqueous solutions. The slow dissolution of the surface silanol layer was the primary cause of the long-term instability of the PEO-modified SiO<sub>2</sub> NPs. Although PEO modification can only keep SiO<sub>2</sub> NPs stable for less than a month, this technique played a crucial role in the surface engineering of SiO<sub>2</sub> NPs. Yoon *et al.* prepared SiO<sub>2</sub>-coated magnetic particles and grafted low molecular weight PEG (polymerization degree of 6 to 9) onto it using a similar method; this process is known as PEGylation.<sup>39</sup> It was accomplished by adding commercially available trimethoxysilane terminated PEG (silane-PEG) to solutions at the end of the synthesis. This method is faster than others because it eliminated the synthesis step of silane-PEG, making it the most widely used method for grafting PEG onto SiO<sub>2</sub> NPs to date. In addition, Wiesner *et al.* demonstrated that the enhanced stability of PEGylation is primarily a result of the increased steric repulsion (Fig. 3a).<sup>40</sup> As the silane-PEG concentration increased, the surface  $\zeta$ -potential decreased while the density of grafted PEG increased, emphasizing the effect of steric hindrance from PEGylation. Based on this strategy, ultrasmall and highly symmetrical SiO<sub>2</sub> cages were first synthesized and reconstructed using cryo-EM single particle 3D reconstruction (Fig. 3b).<sup>37</sup> The PEG surface modification by the addition of silane-PEG resulted in a high degree of size and morphology uniformity.

In light of the potential applications of SiO<sub>2</sub> in organisms, the high concentration of ions in the physiological environment poses new stability challenges. To meet the stringent requirements, the electrostatic repulsive force and steric hindrance must be further increased. Accordingly, the influence of the coverage density and chain length of the PEG polymer on the stability of SiO<sub>2</sub> NPs in simulated body fluid (SBF) was investigated first.<sup>41</sup> They demonstrated that longer ( $M_w$  5000) and denser PEG polymer shells are more effective at slowing the biodegradation kinetics of SiO<sub>2</sub> NPs in SBF. The increased steric hindrance contributed to the enhanced stability. In addition, Tan *et al.* discovered that the carboxylate groups on the surface of SiO<sub>2</sub> NPs exhibited a higher EDL stern plane due to a more electrostatic and steric environment, when combined with octadecyl surface modification (Fig. 3c).<sup>42</sup> This strategy combined electrostatic repulsive force

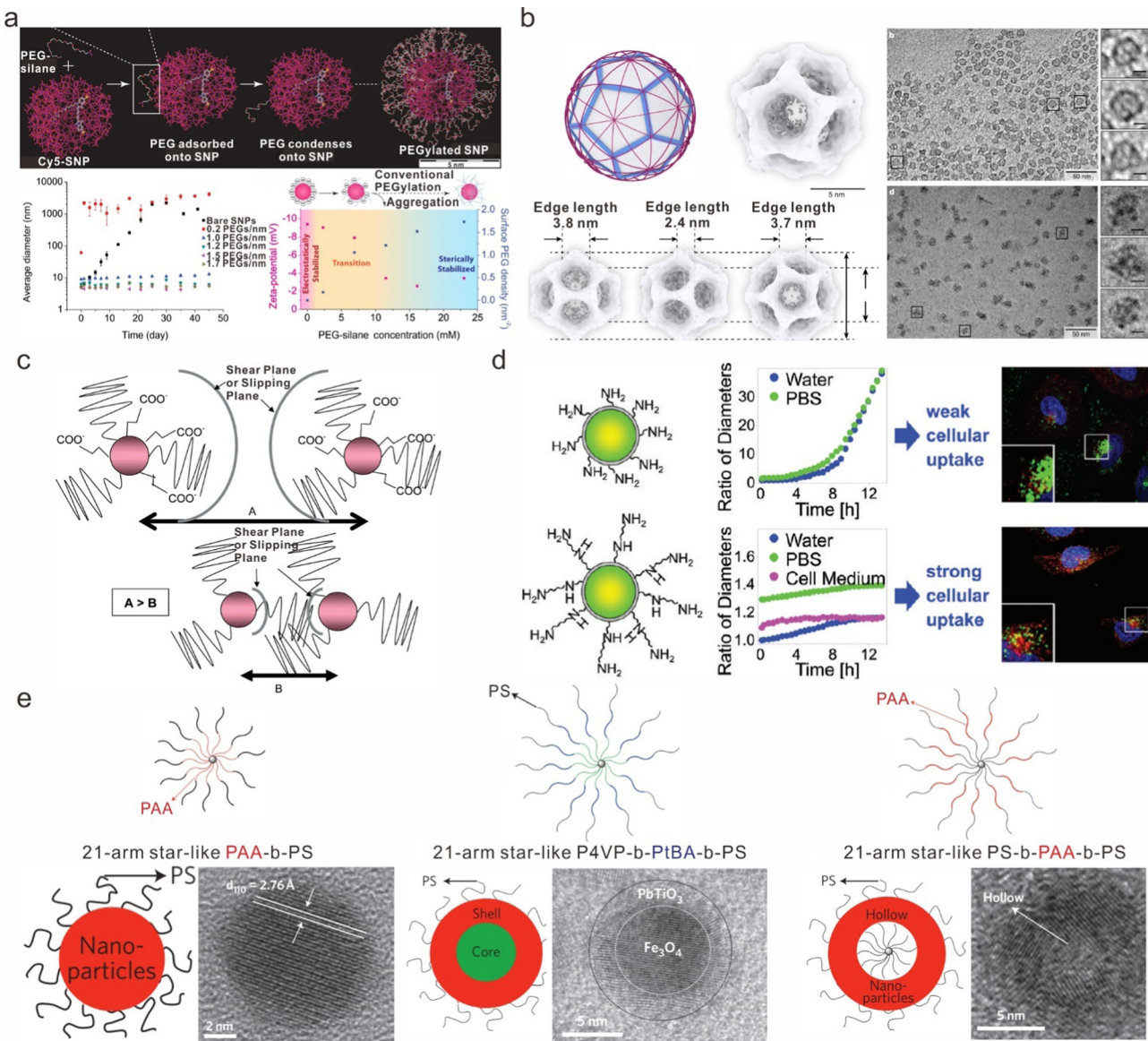


**Fig. 3** Surface engineering of  $\text{SiO}_2$  NPs for colloidal stability. (a) Method of PEGylation on  $\text{SiO}_2$  NPs. The  $\zeta$ -potentials revealed that the role of PEG surface groups is steric repulsion, and not electrostatic repulsion. Reprinted with permission from ref. 40. Copyright 2016 American Chemical Society. (b) Monodisperse cage-like  $\text{SiO}_2$  NPs with PEGylation. Particle aggregation was frequently observed in the absence of PEGylation. Reprinted with permission from ref. 37. Copyright 2018 Springer Nature. (c) Combination of electrostatic repulsive-force and steric hindrance by modifying two different molecule groups. Reprinted with permission from ref. 42. Copyright 2006 American Chemical Society. (d) Positively charged modified surface with long chain methyl groups can improve the dispersity of  $\text{SiO}_2$  NPs in physiological media, and simultaneously increase the cellular uptake of NPs via electrostatic attraction. Reprinted with permission from ref. 18. Copyright 2012 American Chemical Society. (e) Designed block copolymer can self-assemble into spherical micelles that are capped by PS molecules. Nanocrystals grow on PAA segments, while PS molecules inhibit aggregation. Reprinted with permission from ref. 44. Copyright 2013 Springer Nature.

and steric hindrance, exhibiting greater stability than single groups such as carboxyl, C18, and PEG. Additionally, Rühl *et al.* investigated the effect of various surface groups on the colloidal stability of NPs in physiological media (Fig. 3d).<sup>18</sup> They modified the surface of  $\text{SiO}_2$  NPs with amino acids, amino or PEG and tested their stability in physiological media with nearly neutral pH, such as PBS, Tris, RPMI, DMEM, and DMEM + 10% FCS. The  $\zeta$  potential, hydrodynamic diameter, and TEM images all demonstrated that *N*-(6-aminohexyl)-3-aminopropyltrimethoxy silane (AHAPS) and PEG-functionalized  $\text{SiO}_2$  NPs are stable in all media.

Notably, AHAPS stabilized  $\text{SiO}_2$  NPs are more stable in artificial high ionic strength media up to  $0.274 \text{ mol L}^{-1}$  NaCl. The hydrodynamic diameter of AHAPS-stabilized particles was comparable at all NaCl concentrations, whereas the value for PEG-stabilized particles increased threefold.

**Pre-grafting on a designed template.** Pre-grafting on a designed template is another essential surface engineering method. In the shell of block copolymer spheres, an inert polymer [polystyrene (PS)] can be incorporated, which subsequently serves as a template for the growth of colloidal NPs

onto its core. In general, block copolymers can self-assemble into spherical micelles when their concentration in aqueous solution reaches the critical micelle concentration.<sup>43</sup> Typical block copolymers are linear and composed of two or three distinct monomers organized into two to three distinct blocks: AB, ABA, ABC, such as poly(acrylic acid)-*block*-polystyrene (PAA-*b*-PS) and polystyrene-*block*-poly(acrylic acid)-*block*-poly(ethylene oxide) (PS-*b*-PAA-*b*-PEO). In the formed spherical micelles, the PAA polymer can be used to deposit silica, whereas PS segments become inert molecular groups on the surface of SiO<sub>2</sub> NPs leading to steric hindrance. Using star-like block copolymers as templates, Lin *et al.* reported a general strategy for producing a wide variety of functional nanocrystals (Fig. 3e).<sup>44</sup> They enabled the facile synthesis of nearly monodisperse nanocrystals with desired composition and architecture. The steric hindrance resulting from the PS polymer on the surface of the nanocrystals contributes to a high dispersity.

**Co-condensation.** The co-condensation strategy can also be used to engineer the surface of NPs in one-pot reaction.<sup>45</sup> Biocompatible PEG polymers were added to the SiO<sub>2</sub> synthesis systems at an early stage, thereby eliminating the possibility of chemical toxicity. However, for co-condensation, PEG is incorporated into the surface of SiO<sub>2</sub> NPs in an uncontrolled manner. Consequently, an unknown amount of PEG is buried within the particles, making the quantitative determination of the amount of PEG on the surface extremely difficult.

### 2.3 Surface engineering of hydrophobic MNCs for colloidal stability

The magnetic properties of hydrophobic Fe<sub>3</sub>O<sub>4</sub> MNCs are dependent on their composition, shape, and surface engineering. Correspondingly, diverse Fe<sub>3</sub>O<sub>4</sub> synthesis methods, including bottom-up (solution-phase synthesis such as high-temperature decomposition,<sup>46</sup> hydrothermal<sup>47</sup> and solvothermal<sup>48</sup>) and top-down (ball milling) approaches, have been developed.<sup>49</sup> In solution-phase synthesis, a stabilized ligand (oleic acid) with an 18-carbon tail is used to coordinate to Fe<sup>3+</sup> ions during high-temperature decomposition of Fe(Acac)<sub>3</sub> (iron(III) acetyl-acetonate),<sup>32,50</sup> and oleic acid surface modified Fe<sub>3</sub>O<sub>4</sub> MNCs are produced in a nonpolar solvent such as benzyl ether. Importantly, the hydrophobic 18-carbon tail on the surface could destabilize the Fe<sub>3</sub>O<sub>4</sub> MNCs in polar solvents such as aqueous solution,<sup>51,52</sup> making it challenging to prepare biocompatible Fe<sub>3</sub>O<sub>4</sub> MNCs. In this section, two strategies for phase transfer of Fe<sub>3</sub>O<sub>4</sub> MNCs from a nonpolar solvent to an aqueous solution are discussed: amphiphilic ligand encapsulation<sup>53–56</sup> and ligand-exchange.<sup>51,52,57–59</sup> The former uses amphiphilic molecules to coordinate with the original ligands *via* hydrophobic vdW interactions, whereas the latter replaces the original ligands with hydrophilic molecules.

**Amphiphilic ligand encapsulation strategy.** The amphiphilic ligand encapsulation strategy involves binding of the hydrophobic chain of an amphiphilic molecule to oleic acid and exposing the hydrophilic segments, which renders Fe<sub>3</sub>O<sub>4</sub> MNCs water-soluble. Yang *et al.*, as an example, modified the surface properties of Fe<sub>3</sub>O<sub>4</sub> MNCs by forming an  $\alpha$ -cyclodextrin ( $\alpha$ -CD)/

oleic acid complex. The resulting Fe<sub>3</sub>O<sub>4</sub> MNCs are stable in water under ambient atmospheric conditions for extended durations (Fig. 4a).<sup>53</sup> Moreover, water-soluble AuNPs, Fe<sub>3</sub>O<sub>4</sub> MNCs, and CdSe/ZnS QDs were manufactured using “dual interaction ligands” with both hydrophilic and hydrophobic chain segments (Fig. 4b).<sup>55</sup> The resulting NP-ligand complex exhibited exceptional stability over a broad pH range, at high salt concentrations, and in thermal treatment up to 100 °C. In addition, fatty acid can adsorb onto the surface of Fe<sub>3</sub>O<sub>4</sub> MNCs and form a bilayer structure, transferring hydrophobic Fe<sub>3</sub>O<sub>4</sub> into an aqueous phase (Fig. 4c).<sup>56</sup> Nevertheless, the amphiphilic ligand encapsulation strategy was typically carried out in two phases: Fe<sub>3</sub>O<sub>4</sub> MNCs in the hydrophobic phase, and amphiphilic molecules in the hydrophilic phase. When combined with polar solvents, Fe<sub>3</sub>O<sub>4</sub> MNCs tended to aggregate prior to encapsulation by an amphiphilic ligand, resulting in poor phase transfer efficiency.

**Ligand-exchange strategy.** In contrast to the amphiphilic ligand encapsulation strategy, the ligand-exchange method forms a new ligand-Fe<sub>3</sub>O<sub>4</sub> complex through covalent bonding, which is more stable in an aqueous phase. Cheon *et al.* fabricated water-soluble thiol-modified Fe<sub>3</sub>O<sub>4</sub> MNCs by dissolving 2,3-dimercaptosuccinic in dimethyl sulfoxide (DMSO) and adding it to nonpolar toluene containing Fe<sub>3</sub>O<sub>4</sub>.<sup>57</sup> Based on this result, they created core-satellite dye-doped SiO<sub>2</sub>-(Fe<sub>3</sub>O<sub>4</sub>)<sub>n</sub> NPs, indicating that the monodisperse thiol-modified MNCs in water can be further manipulated in a controlled way (Fig. 4d).<sup>58</sup> By exchanging the oleic acid ligand with multicharged ions (amino alkane, R-NH<sub>2</sub> or carboxyl alkane, R-COOH), Tan *et al.* transferred various types of hydrophobic MNCs including FePt, Fe<sub>3</sub>O<sub>4</sub>, Pd, CdSe, and NaYF<sub>4</sub> to an aqueous phase (Fig. 4e).<sup>51,52</sup> The as-transferred MNCs can be further surface functionalized with small molecule dyes, oligonucleotides, and enzymes, significantly expanding the applications of hydrophobic NPs in water. In addition, Murray *et al.* developed a reversible phase transfer strategy between hydrophobic and hydrophilic media for various hydrophobic MNCs (metal oxides, metals, semiconductors, and dielectrics) (Fig. 4f),<sup>59</sup> in which the oleic acid ligand was replaced with nitrosonium tetrafluoroborate (NOBF<sub>4</sub>). This enabled MNCs to remain stable in water for years, which exceeded their initial solubility in nonpolar solvents. Furthermore, due to the weak binding affinity of BF<sup>−</sup> anions to the MNCs surface, the obtained hydrophilic MNCs are amenable to reversed surface molecule exchange with diverse capping molecules.

In addition to enhancing the stability of particles in water, surface engineering can control the intracellular aggregation of Fe<sub>3</sub>O<sub>4</sub> MNCs and improve T2 magnetic resonance imaging (MRI) in tissues. Liang *et al.* designed a small molecule Ac-Asp-Glu-Val-Asp-Cys(StBu)-LysCBT (1), which covalently attaches to USPIO NPs producing a monodispersed Fe<sub>3</sub>O<sub>4</sub>@1 complex.<sup>60</sup> Caspase 3 is able to recognize intracellular aggregation of Fe<sub>3</sub>O<sub>4</sub>@1 complexes *in vivo*, which can be utilized to enhance T2 MRI imaging of tumor apoptosis. Similarly, Gao *et al.* reported GSH-induced Fe<sub>3</sub>O<sub>4</sub> aggregation *in vivo* and demonstrated enhanced MRI contrast enhancement performance.<sup>7</sup> The surface of the imaging probe was capped with a PEG ligand

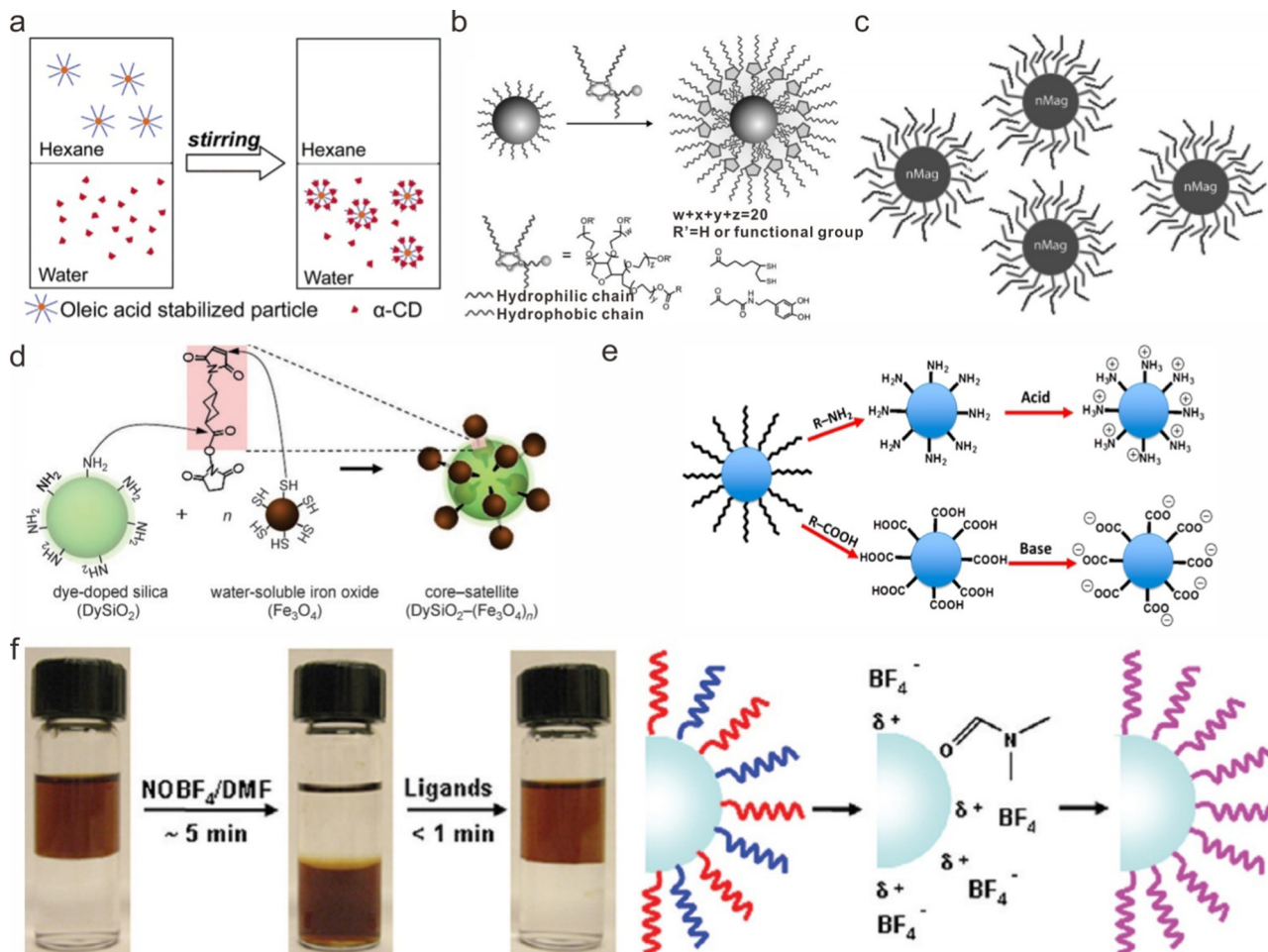


**Fig. 4** Surface engineering of hydrophobic MNCs for colloidal stability. (a)–(c) Amphiphilic ligand encapsulation strategy: (a)  $\alpha$ -CD Reprinted with permission from ref. 53. Copyright 2003 American Chemical Society. (b) Dual interaction ligands. Reprinted with permission from ref. 55. Copyright 2008 John Wiley and Sons. (c) Fatty acid. Reprinted with permission from ref. 56. Copyright 2009 American Chemical Society. (d) and (e) Ligand-exchange strategy: (d) thiol. Reprinted with permission from ref. 58. Copyright 2006 John Wiley and Sons. (e) Amine and carboxyl. Reprinted with permission from ref. 52. Copyright 2015 American Chemical Society. (f) General, fast and reversible ligand-exchange strategy for various MNCs (metal oxides, metals, semiconductors and dielectrics). Reprinted with permission from ref. 59. Copyright 2011 American Chemical Society.

composed of an RGD peptide and a self-peptide sequence. After GSH-induced cleavage of the self-peptide portion within the tumor, *in situ* cross-linking and aggregation of the responsive probes were performed.

#### 2.4 Surface engineering of CNTs for colloidal stability

CNTs are excellent nanomaterials for cellular delivery, fluorescent imaging, nanosensors and disease diagnosis. However, the high vdW attractive force could lead to severe CNT aggregation in the majority of solvents, which greatly hinders the manipulation of CNTs.<sup>5</sup> To improve the dispersity of CNTs in solvents, a number of methods focusing on surface engineering on CNTs have been reported, typically comprising (1) covalent sidewall chemistry; (2) non-covalent surfactant encapsulation; and (3) non-covalent polymer wrapping.

**Covalent sidewall chemistry.** The  $\pi$ – $\pi$  stacking interaction and vdW force of CNTs can be easily overcome by surface engineering based on covalent sidewall chemistry. At various temperatures, Margravea *et al.* demonstrated that fluorine can

be covalently attached to the sidewall of CNTs.<sup>61</sup> In addition to their enhanced stability, CNTs with a fluoride group on the surface exhibited greater reaction activity than bare CNTs, and can therefore be further functionalized by nucleophilic substitution. For instance, the C–F atomic bond on fluorinated CNTs can be attacked and replaced by nucleophilic agents (*e.g.*, urea), producing urea-functionalized CNTs (Fig. 5a).<sup>62</sup> Compared to fluorinated CNTs, the urea-functionalized CNTs showed higher stability in DMF, water, and aqueous urea solutions.

**Non-covalent surfactant encapsulation.** Despite the aforementioned benefits, covalent sidewall chemistry frequently induces irreversible alterations in the intrinsic properties of CNTs. As opposed to covalent chemistry, non-covalent chemistry can reduce surface modification's detrimental effects. For instance, surfactants such as sodium dodecyl sulfate (SDS) can debundle and disperse CNTs in solutions *via* non-covalent surfactant encapsulation (Fig. 5b).<sup>63</sup> SDS wraps the CNTs through hydrophobic/hydrophilic interaction, in which the

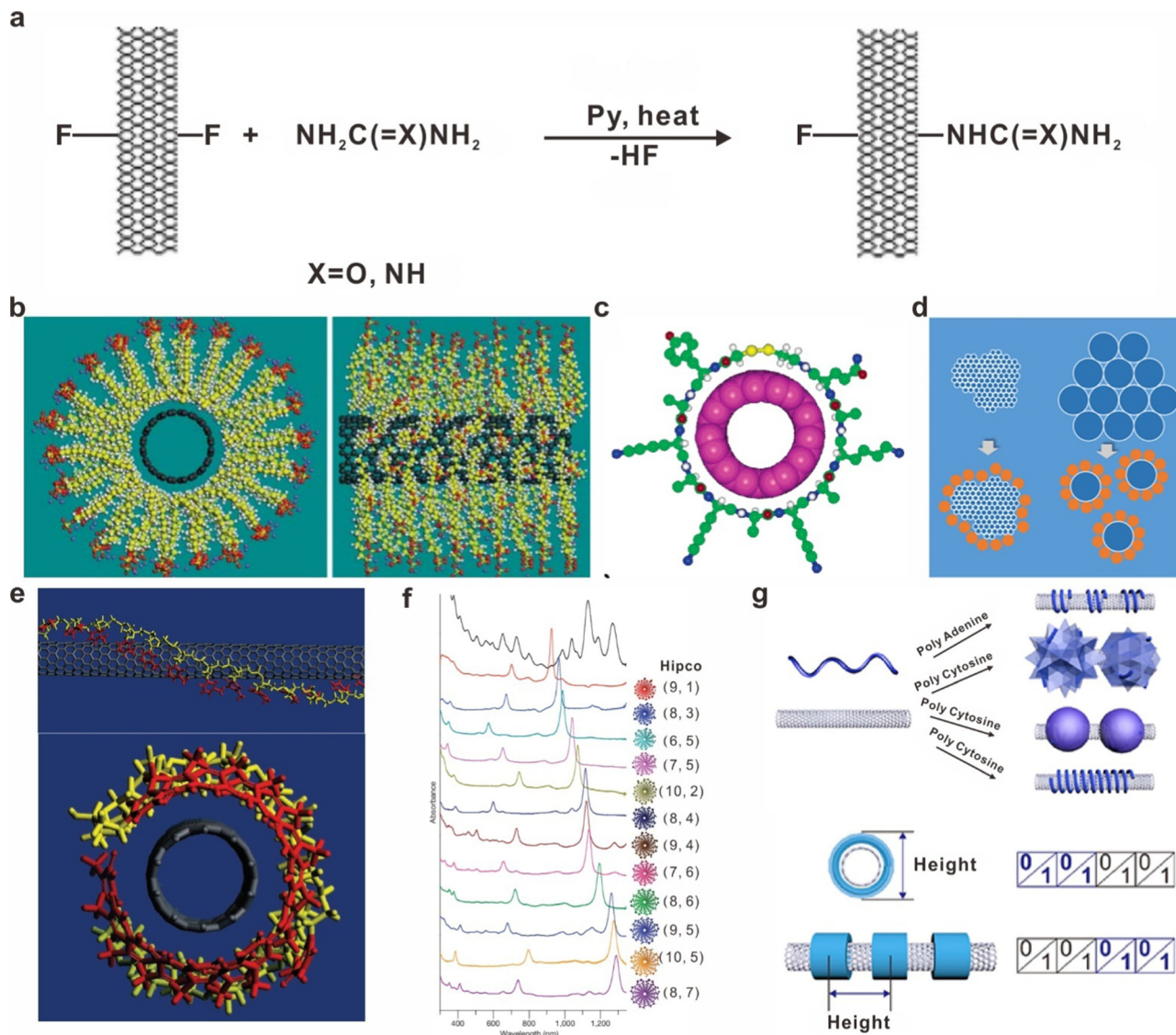


**Fig. 5** Surface engineering of CNTs for colloidal stability. (a) Surface fluorination of CNTs and their subsequent functionalization based on the covalent sidewall chemistry. Reprinted with permission from ref. 62. Copyright 2008 American Chemical Society. (b) Wrapping of SDS on CNTs. Reprinted with permission from ref. 63. Copyright 2010 Royal Society of Chemistry. (c) Wrapping of RCPs peptides on CNTs. Reprinted with permission from ref. 66. Copyright 2005 American Chemical Society. (d) Wrapping of C1q protein on CNTs. Reprinted with permission from ref. 67. Copyright 2017 American Chemical Society. (e) Wrapping of DNA on CNTs. Reprinted with permission from ref. 71. Copyright 2003 Springer Nature. (f) DNA facilitates the selective separation of CNTs in synthetic mixtures. Reprinted with permission from ref. 73. Copyright 2009 Springer Nature. (g) Tubular nucleic acids can be used to encode CNTs for information storage. Reprinted with permission from ref. 75. Copyright 2019 American Chemical Society.

hydrophobic tails of SDS penetrate the space between adjacent CNTs and adsorb on CNTs. The hydrophilic heads extend into the aqueous solution and consequently enhance the dispersibility of CNTs. In addition, peptides, proteins, and streptavidin can adsorb on the surface of CNTs to increase their dispersibility.<sup>64,65</sup> For instance, reversible cyclic peptides (RCPs) can envelop CNTs and form closed rings *via* head-to-tail covalent bonds, thereby achieving diameter-selective solubilization of CNTs (Fig. 5c).<sup>66</sup> Moreover, the protein C1q can disaggregate bundles of large diameter multiwalled CNTs selectively, but not those of thin single-walled CNTs (Fig. 5d).<sup>67</sup> In addition, Tour *et al.* demonstrated that substituted aniline can also functionalize CNTs through non-

covalent interactions.<sup>68</sup> The functionalized CNTs can be diluted with various organic solvents (*e.g.*, DMF, acetone) without aggregation.

**Non-covalent polymer wrapping.** Based on the  $\pi-\pi$  stacking forces between DNA bases and CNTs, DNA wrapping has been shown to be a site-selective, easily implemented, and widely applicable method for dispersing CNTs.<sup>69,70</sup> Single-stranded DNA (ssDNA) could interact strongly with CNTs to form a stable DNA–CNT complex, resulting in the homogenous dispersion of CNTs in an aqueous solution (Fig. 5e).<sup>71</sup> More importantly, the wrapping of DNA on CNTs is sequence-dependent; therefore, it can be used for DNA-based CNT separation.<sup>72</sup> Subsequently,

researchers confirmed this hypothesis and discovered that different forms of CNTs in synthetic mixtures can be recognized and purified through sequence- and length-dependent interactions with DNA and CNTs (Fig. 5f).<sup>73</sup> In addition, handedness and helicity of CNTs can also be recognized using homochiral DNA with a specific sequence.<sup>74</sup>

In addition to promoting the separation of CNTs, sequence-dependent interactions between ssDNA and CNTs can also influence the conformation of ssDNA on CNTs. Zuo *et al.* studied the interactions between CNTs and ssDNA, and observed sequence-specific ssDNA conformations on CNTs, such as helices, i-motifs, and G-quadruplexes (Fig. 5g).<sup>75</sup> When adsorbed on CNTs, poly-A encoded ssDNA formed an ordered helix structure, whereas poly-G encoded ssDNA aggregated into large DNA clumps. Therefore, CNTs can be encoded for information storage by tubular nucleic acids based on this distinction.

### 3 Self-assembly of colloidal NPs

In addition to inhibiting the random aggregation of colloidal particles, surface functional groups can agglomerate well-dispersed colloids in a controlled manner, which is typically referred to as self-assembly of NPs. Self-assembly affords new possibilities for the preparation of functional materials with desirable properties. These remarkable superstructures enable the processing of hierarchically more complex materials. Diverse short- and long-range interactions, such as electrostatic forces, steric repulsion, van der Waals force, entropic force, depletion force, molecular dipole interactions, capillary force, hydrogen bonding, capillary force, and surface patchy interaction, contribute to the self-assembly of NPs.<sup>76,77</sup> In response to these interactions, examples of self-assembled structures include DNA,<sup>78</sup> proteins,<sup>79</sup> lipid vesicles,<sup>80</sup> block copolymer melts<sup>81</sup> and inorganic NPs.<sup>82,83</sup> By evaporating solvents, for instance, ordered arrays of colloidal NPs superlattices can be created; this process is known as evaporation-induced self-assembly (EISA).<sup>6</sup> EISA typically follows the entropy maximization principle for hard particles and occurs in the final phase of solvent drying. Colloidal NPs could find themselves in crowded solutions, resulting in the formation of a superlattice film at the air-liquid interface. Accordingly, a small volume of diluted NP solution was experimentally deposited on a solid support and allowed to dry for a couple of minutes.<sup>84</sup> Similarly, polar liquids (*e.g.*, diethylene glycol) combined with immiscible nonpolar solvents have also been used as a platform for NP assembly. This technique yields extended superlattice thin films on solvents that can be transferred to solid supports for subsequent applications.<sup>85</sup>

Another qualitatively distinct method for the self-assembly of colloidal NPs employs particles with programmable interactions through DNA linkers.<sup>86–91</sup> With the development of surface oligonucleotide modification with desired sequences onto various NPs, the application of DNA as structure-directing surface groups has become an important research topic in the field of self-assembly. Here, we examine the emergence of DNA-directed NP assembly strategy. For other self-

assembly strategies, the existing literature should be consulted.<sup>76,92</sup>

#### 3.1 Highly dense DNA conjunction onto colloidal NPs

DNA has evolved into a programmable tool for assembling NPs into a variety of ordered structures.<sup>86,87</sup> Experimentally, it consists of two steps: the attachment of DNA to colloidal NPs and the DNA hybridization-induced self-assembly of the NPs–DNA complex. For the first step, people have developed a variety of quick and effective methods for various colloidal NPs. AuNPs are the most common NPs utilized for DNA-directed self-assembly. The critical step in attaching thiol (SH)-DNA to AuNPs *via* Au–S bonding is the reduction of the distance between DNA and AuNPs in aqueous solution. Representative methods include salting-aging, lowering pH, freezing, instant dehydration in butanol and microwave-assisted heating-drying.

The salting-aging induced DNA attachment is the most universal method for binding SH-DNA to variously shaped AuNPs, such as spheres, rods, and triangles (Fig. 6a).<sup>93,94</sup> In an aqueous solution, citrate-stabilized AuNPs are mixed with thiol-DNA to form a low-density packing of DNA on the surface. A high-density DNA shell is formed by adding high concentrations of salt (typically NaCl) to the mixture and incubating it for over ~12 h. In the process of salting aging, a high concentration of salt reduces the EDL thickness and, consequently, the repulsive force between DNA and AuNPs. However, a too rapid increase in ionic strength will result in the severe aggregation of AuNPs, making salting aging difficult and time-consuming to process. Additional disadvantages, such as DNA waste and multiple procedures, further complicate this method. An efficient and cost-effective method is essential. Focusing on these issues, people devised a new method for reducing the electrostatic repulsion between DNA and AuNPs by lowering pH to 3.0 rather than by increasing ionic strength (Fig. 6b).<sup>95</sup> When the pH is less than the isoelectric point, A and C bases acquire a positive charge, and citrate on AuNPs is partially protonated, thereby facilitating rapid adsorption (only several minutes). In addition, the method achieved multiplexed DNA functionalization with precise density control, enabling the adsorption of a specified number of DNA molecules. However, precise control of pH still requires a delicate experimental procedure, particularly for small volumes.

To further simplify surface oligonucleotide modification, people have developed a super convenient method that involves simply freezing and melting a DNA/AuNP solution (Fig. 6c).<sup>96,97</sup> In a few minutes, DNA–AuNPs are formed during the freezing–melting process without the addition of any extra reagents. This method increases DNA density by 20–30% compared to the previous salt-aging method and is applicable to AuNPs of various sizes (5–100 nm). Instead of adjusting the electrostatic repulsion, it was discovered that freezing methods reduce the distance between DNA and AuNPs through a crowding effect. When the temperature drops to extremely low levels, ice crystals form in the solution, condensing the AuNPs, DNA, and salt in a small space. This significantly increases the DNA concentration surrounding AuNPs and accelerates the Au–S bonding rate.

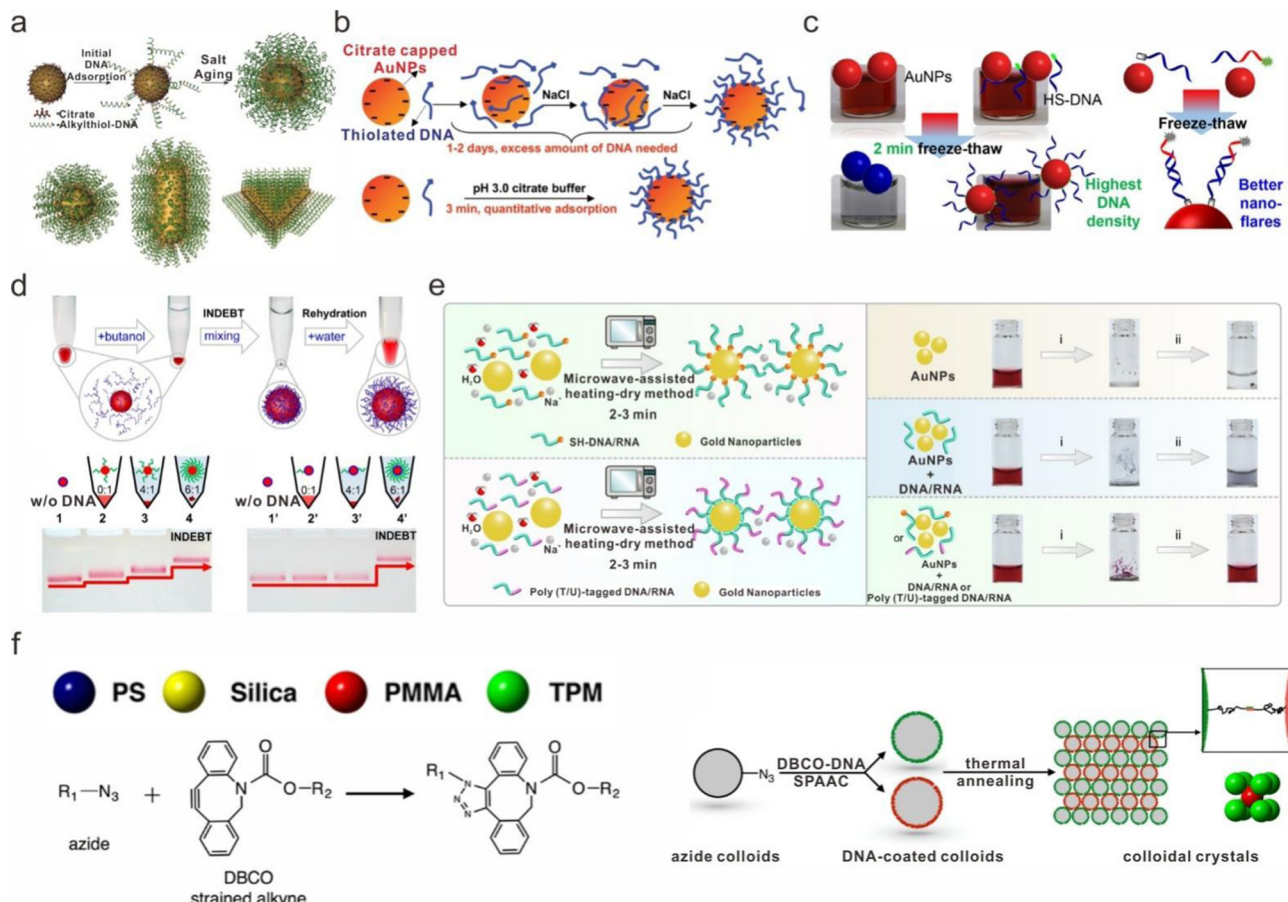


**Fig. 6** Highly dense DNA conjunction onto colloidal NPs. (a) and (b) Two representative methods for binding DNA on AuNPs by decreasing the electrostatic repulsive force. (a) salting–aging method. Reprinted with permission from ref. 93. Copyright 2012 American Chemical Society. (b) Precise control of pH method. Reprinted with permission from ref. 95. Copyright 2012 American Chemical Society. (c)–(e) Binding of DNA on AuNPs using a crowding effect. (c) Freezing and melting of the DNA/AuNPs. Reprinted with permission from ref. 96. Copyright 2017 American Chemical Society. (d) Butanol-based dehydration strategy. Reprinted with permission from ref. 98. Copyright 2021 American Chemical Society. (e) Microwave (MW)-assisted heating-dry method. Reprinted with permission from ref. 99. Copyright 2022 Springer Nature. (f) General method for DNA binding on various NPs including poly(styrene), poly (methyl methacrylate), titania, and silica by mixing DBCO-DNA with azide-functionalized NPs. Reprinted with permission from ref. 100. Copyright 2015 American Chemical Society.

Similarly, dehydration in butanol enabled the instant synthesis of DNA–AuNP complexes with record-high DNA concentration in seconds (Fig. 6d).<sup>98</sup> This butanol-based strategy relies on rapid removal of water from the DNA/AuNP mixture to produce a dehydrated “solid solution” that concentrates SH-DNA and AuNPs to their maximum concentration. The ultrafast experimental procedure and superdense DNA grafting make this method highly superior to previous ones. Recent reports indicate that non-thiolated DNA/RNA can be conjugated to AuNPs using a microwave (MW)-assisted heating-dry method (Fig. 6e).<sup>99</sup> CRISPR/Cas9-sgRNA (136 bp), SARS-CoV-2 RNA fragments (1278 bp), and rolling circle amplification (RCA) DNA products (over 1000 bp) have been successfully attached to AuNPs, showing great promise for biosensing and nucleic acid delivery applications. The mechanism of this strategy is similar to the freezing–melting method and the butanol-based method, in which the instantaneous high concentration of DNA is a critical factor.

Pine *et al.* reported a general DNA binding strategy for colloidal NPs with a variety of chemical compositions, such

as poly(styrene), poly(methyl methacrylate), titania, and silica (Fig. 6f).<sup>100</sup> Using a strain-promoted alkyne–azide cycloaddition reaction, single-stranded oligonucleotides were covalently grafted onto particle surfaces.

### 3.2 Anisotropic DNA conjunction onto colloidal NPs

Although the functionalization of AuNPs with SH-DNA is a mature method and has been widely used in numerous fields, such as biosensing, optics, electricity, and nanomedicine, it is incapable of providing anisotropic surface binding of ssDNA. Therefore, constructing NP assemblies with programmable configurations is challenging. Sleiman *et al.* reported a molecular printing technique in which the AuNPs can inherit the DNA sequence configuration encoded in the parent template, exhibiting site-specific addressability with complex numbers, geometry, and placement (Fig. 7a).<sup>101</sup> The high affinity between poly-adenine (poly-A) and AuNPs is an additional important anisotropic DNA binding strategy. Utilizing single-stranded DNA encoders, people created programmable colloidal atoms

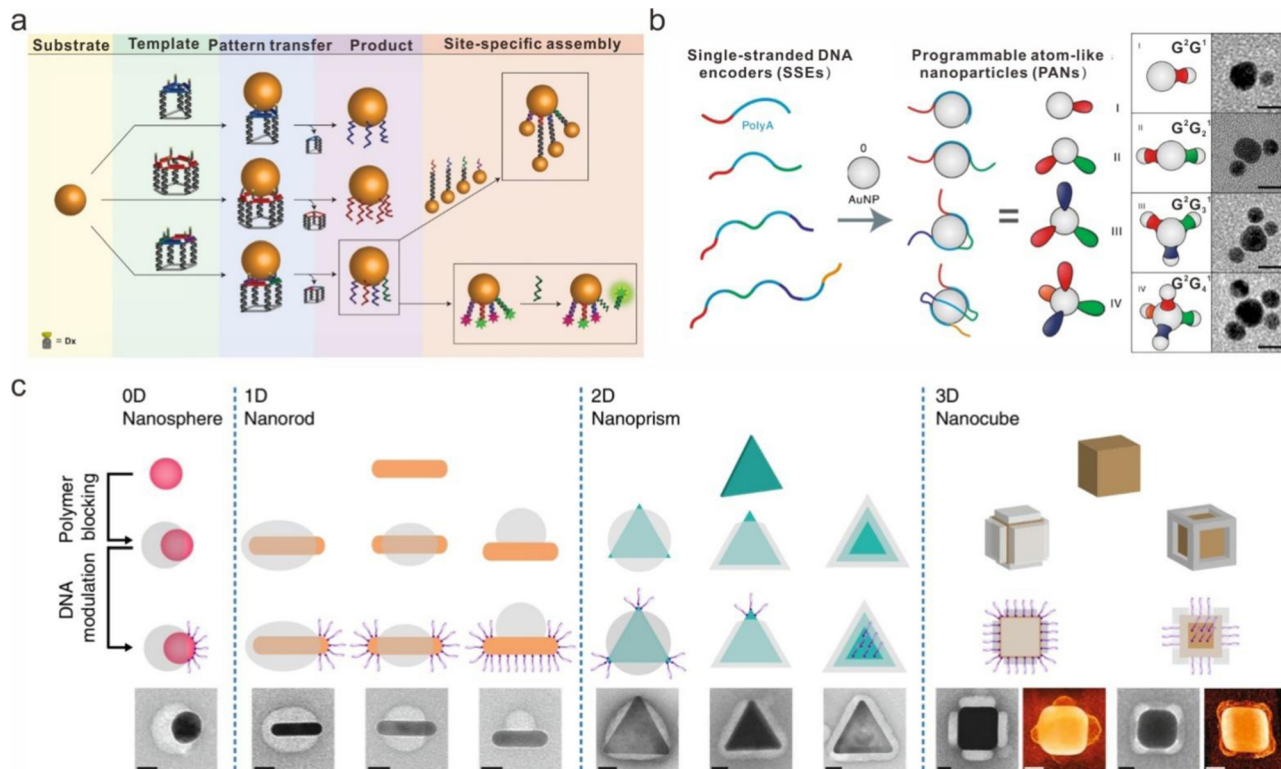


**Fig. 7** Anisotropic DNA conjunction onto colloidal NPs. (a) Molecular printing strategy for encoding anisotropic DNA on AuNPs. Reprinted with permission from ref. 101. Copyright 2016 Springer Nature. (b) Poly-adenine (poly-A) mediated programmable atom-like NPs (PANs). Reprinted with permission from ref. 102. Copyright 2019 Springer Nature. (c) Regioselective surface DNA binding onto anisotropic NPs. Reprinted with permission from ref. 103. Copyright 2018 Springer Nature.

with a valence bond and colloidal molecules of various compositions, sizes, and structures (Fig. 7b).<sup>102</sup> Besides the isotropic gold NPs, Weizmann *et al.* developed a regioselective surface DNA binding method on anisotropic gold NPs by blocking surfaces selectively with a diblock copolymer (Fig. 7c).<sup>103</sup> This strategy demonstrated good adaptability for various NPs with isotropic and anisotropic shapes, and allowed for a higher degree of potential self-assembly complexity.<sup>104</sup>

Another distinct method to construct anisotropic nanoparticles employed Janus NPs, which showed an asymmetric chemical composition and surface.<sup>105</sup> The most common Janus particles are double-faced AuNPs that are suitable for construction of optical probes and asymmetric assembly of bricks.<sup>106</sup> Recently, DNA has been used to explore the design and assembly of Janus NPs with programmable directionality.<sup>107</sup> Lu *et al.* reported a DNA-directed approach to assemble Janus NPs to form asymmetric nanoclusters. Different types of DNA including cDNA and iDNA can be used to control the assembly and disassembly of nanoclusters.<sup>108</sup> They also revealed a size-dependent theory that various asymmetric nanoclusters can be designed and adjusted using programmable base-pairs and NPs of different sizes. Yan *et al.* proposed a Janus NP consisting of two surfaces modified by different DNA strands.<sup>109</sup> Using a method of identifying hierarchical crystallographic assembly, primary crystalline structures (FCC NPs) and secondary crystalline structures (SC, P4 and L NPs) were produced by the

rotational orientation DNA-Janus NPs. They determined the crystallization kinetics of anisotropic NPs by simulations and theoretical analysis.

### 3.3 Framework DNA directed self-assembly of colloidal NPs

To achieve self-assembly of DNA–NP complexes into an ordered structure, up to now, two typical strategies have been developed: DNA hybridization-based assembly and NP-templated assembly.<sup>86</sup> A representative method for realizing DNA hybridization-based assembly of colloidal NPs is based on the framework DNA technique, in which ssDNA strands are first folded into arbitrary 2D and 3D shapes and then served as a scaffold for NP assembly. Due to their unique site addressability, framework DNA, such as DNA origami, single-strand tile (SST) structures, and DNA crystals, enables nanometer-precise organization of organic molecules and inorganic particles in space. In 2006, Rothemund introduced the concept of DNA origami, which relies on the folding of long scaffold strands and hundreds of staple strands (Fig. 8a).<sup>110</sup> The typical DNA origami structures have a diameter of approximately 100 nm and a spatial resolution of 6 nm, with nearly arbitrary shapes. Additionally, individual DNA origami can be programmed to form larger, micrometer-scale assemblies. Due to high assembly yields, precise control over size and shape, and a pixel size of 6 nm for each oligonucleotide, DNA origami is ideally suited to assemble NPs with complex patterns such as chirality and

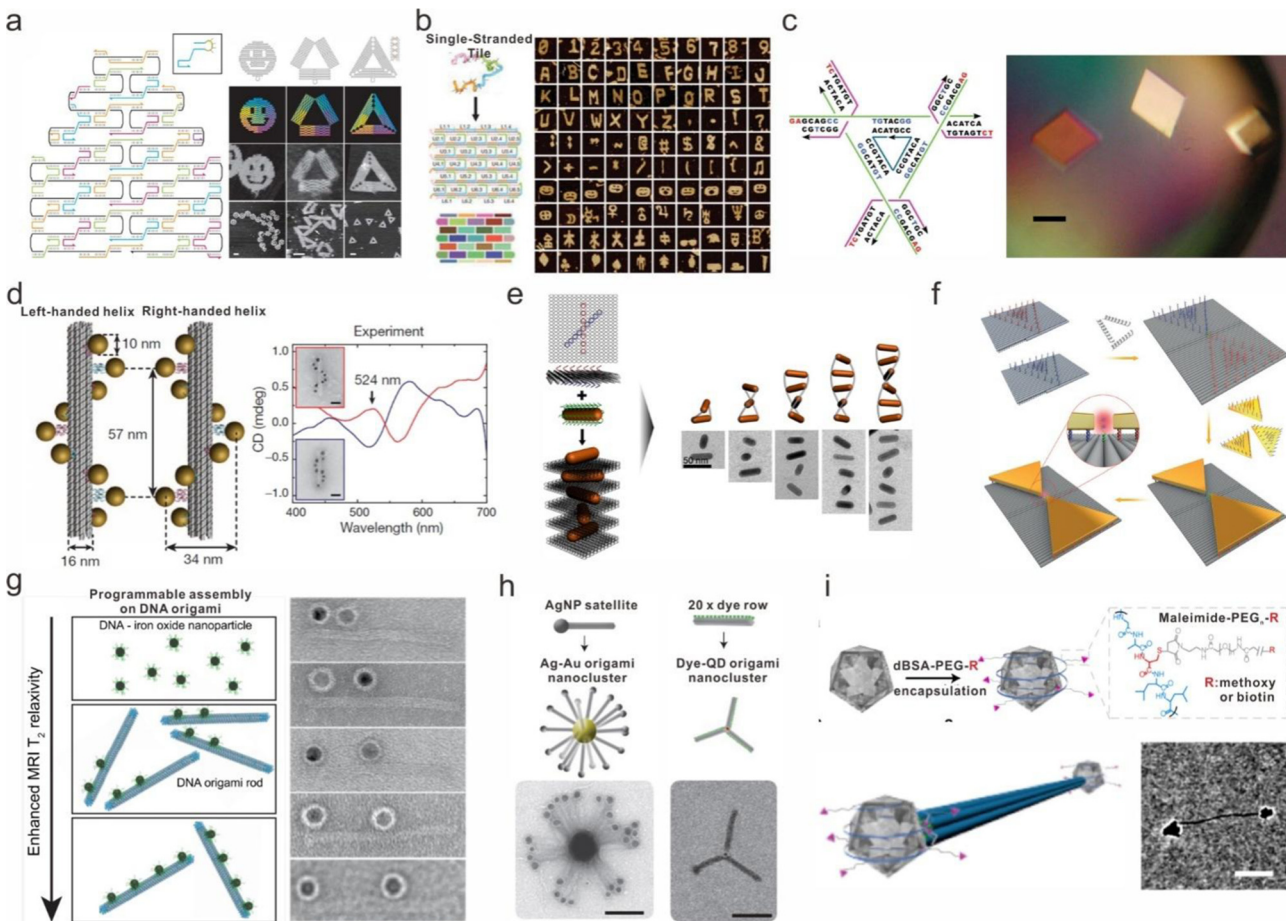


**Fig. 8** Framework of DNA directed self-assembly of colloidal NPs. (a)–(c) Representative DNA self-assembly strategies for fabricating framework of DNA structures: (a) DNA origami. Reprinted with permission from ref. 110. Copyright 2006 Springer Nature. (b) Single-strand tile. Reprinted with permission from ref. 111. Copyright 2012 Springer Nature. (c) DNA crystals. Reprinted with permission from ref. 112. Copyright 2009 Springer Nature. (d)–(f), DNA origami directed assembly of AuNPs with different shapes. (d) AuNP helix architectures formed by attaching to the surface of 24 helix bundles origami. Reprinted with permission from ref. 113. Copyright 2012 Springer Nature. (e) Self-assembly of AuNRs helices templated by 2D DNA origami. Reprinted with permission from ref. 114. Copyright 2015 American Chemical Society. (f) DNA origami directed Au nano prisms assembly. Reprinted with permission from ref. 115. Copyright 2018 John Wiley and Sons. (g)–(i) DNA origami directed assembly of other NPs. (g) Fe<sub>3</sub>O<sub>4</sub>. Reprinted with permission from ref. 21. Copyright 2020 American Chemical Society. (h) AgNPs. Reprinted with permission from ref. 116. Copyright 2013 Springer Nature. (i) Nanodiamonds. Reprinted with permission from ref. 117. Copyright 2015 American Chemical Society.

periodic lattices with nanometer precision. Similar to DNA origami, the SST technique is a complementary method for constructing DNA structures with complex shapes *via* the self-assembly of small monomers (Fig. 8b).<sup>111</sup> Due to the absence of scaffold strands, the SST design does not adhere to the raster fill pattern, allowing for a convenient adjustment in size and shape. In addition, the high periodicity of SST enables the growth of various DNA crystals with micrometer-sized lateral dimensions and depths being precisely controlled to 80 nm. Furthermore, a well-ordered macromolecular 3D nucleic acid crystalline lattice was produced by using a robust tensegrity triangle as a unit (Fig. 8c).<sup>112</sup> Correspondingly, their applications, as foreseen by Nadrian C. Seeman, include the organization of nanoelectronics and the scaffolding of biological systems for crystallographic structure determination.

The construction of various NP architectures, including AuNPs, AuNRs, Au triangular plates, AgNPs, QDs, Fe<sub>3</sub>O<sub>4</sub>, and

nanodiamonds, with the aid of DNA scaffolds demonstrates the power of structural DNA nanotechnology. Kuzyk *et al.* reported in their seminal work on AuNP self-assembly that plasmonic AuNP architectures with LH and RH helical forms were synthesized which exhibited characteristic bisignate signatures in the visible spectrum (Fig. 8d).<sup>113</sup> Through hybridization of extended strands on DNA origami and complementary strands on AuNPs, nine AuNPs were attached to the surface of twenty-four helix DNA bundles. Using comparable procedures, a type of LH- or RH-AuNR helices was formed using 2D rectangular DNA origami (Fig. 8e).<sup>114</sup> The capture strands were arranged on both sides of DNA origami to induce a one-pot chiral assembly of AuNRs. Correspondingly, the DNA origami-directed assembly of Au nanoprisms resulted in the formation of plasmonic bowtie nanostructures consisting of two metallic triangles separated by a 5 nm gap (Fig. 8f).<sup>115</sup> The capture strands were extended from 2D DNA origami in two triangle patterns,

resulting in the precise assembly of Au triangles and giving rise to single-molecule surface-enhanced Raman scattering (SM-SERS).

In addition to the various forms of AuNPs, DNA origami can direct the assembly of  $\text{Fe}_3\text{O}_4$  MNCs, AgNPs, QDs, and nanodiamonds into various superstructures *via* DNA hybridization, resulting in properties that surpass those of single NPs (Fig. 8g–i).<sup>21,116,117</sup>

### 3.4 DNA directed colloidal NP superlattices

Using an alternative technique (NP-templated assembly) for the programmable assembly of NPs, Chad Mirkin, Oleg Gang, and others have developed a vast array of superior crystalline assemblies. Gang *et al.* created three-dimensional crystalline assemblies of AuNPs through interactions between complementary DNA molecules attached to the surface of the NPs. The lengths of the spacer and linker oligonucleotides on NPs had a temperature-dependent effect on the self-assembly of body-centered-cubic (BCC) lattice structures.<sup>118</sup> Mirkin *et al.* created assembled superlattices of AuNPs with various lattice types in the same year.<sup>119</sup> They introduced a series of sequence- and length-specific DNA linkers as structure-directing molecules to form close-packed face-centered-cubic (FCC) and body-centered-

cubic (BCC) superstructures. Two-dimensional small-angle X-ray scattering (SAXS) data collected from the resulting superstructures revealed an ordered and specific structure through scattering patterns. In addition, they presented six design rules that can be used to regulate crystallographic parameters such as particle size (5 to 60 nanometers), periodicity, and inter-particle distance (Fig. 9a).<sup>120</sup> Later, methods to assemble anisotropic NPs into superlattices, including size and shape complementarity, were developed (Fig. 9b).<sup>121,122</sup> After achieving the assembly of isotropic or anisotropic NPs, a low-symmetry crystalline phase was created by co-assembly of atom equivalents (NPs functionalized with a large number of DNA strands) and mobile electron equivalents (small particles functionalized with a low number of DNA strands complementary to the programmable atom equivalents) (Fig. 9c).<sup>123</sup> The corresponding electron equivalents are 1.4 nm AuNPs, which represent the smallest unit utilized in DNA-induced self-assembly.

Self-assembly of NPs induced by DNA origami is another effective method for generating ordered NP superlattices. The DNA origami–NP systems, which consist of polyhedral cage-like DNA origami with anchored NPs inside or on the vertex, become new self-assembly building blocks. Gang *et al.* utilized

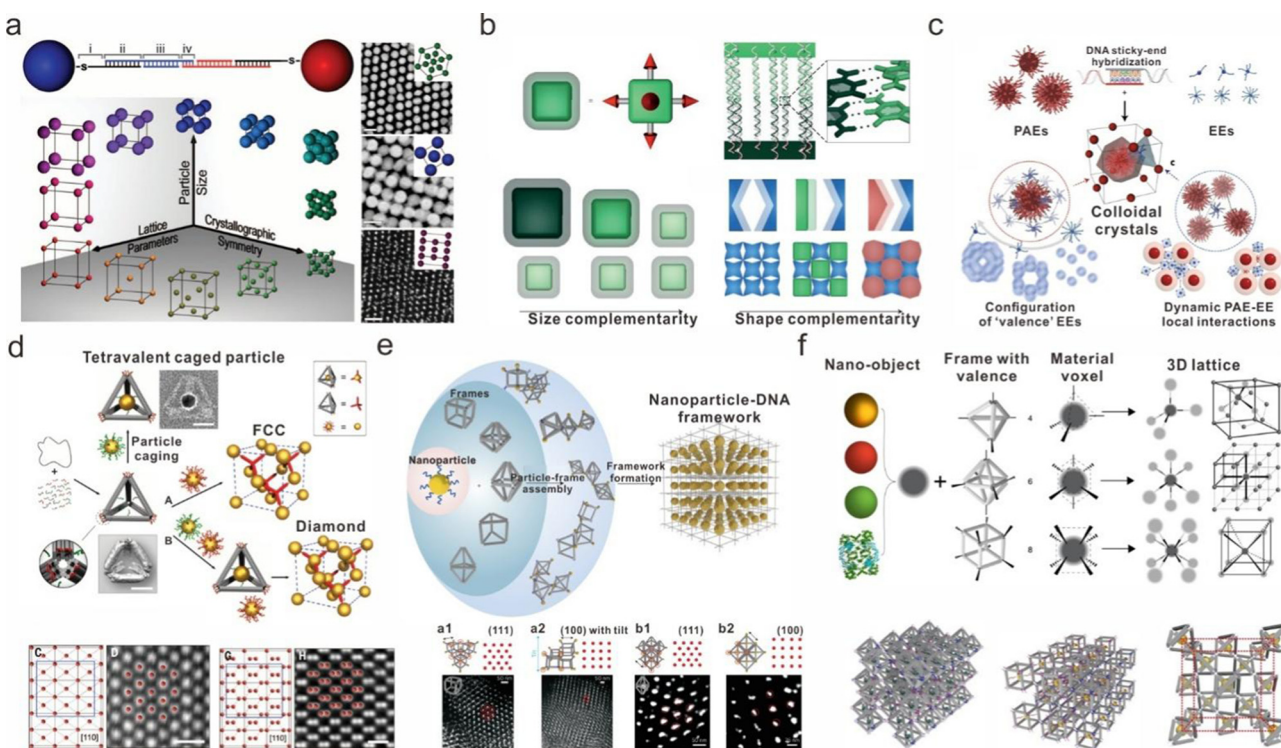


**Fig. 9** DNA directed colloidal NPs superlattices. (a) Isotropic NPs assembled into superlattices by adjusting parameters, including particle size, periodicity, and inter-particle distance. Reprinted with permission from ref. 120. Copyright 2011 The American Association for the Advancement of Science. (b) Anisotropic NPs assembled into superlattice by size complementarity and shape complementarity. Reprinted with permission from ref. 122. Copyright 2015 Springer Nature. (c) Low-symmetry crystalline phase created by co-assembly of atom equivalents (NPs functionalized with many DNA strands) and mobile electron equivalents (small particles functionalized with a low number of DNA strands complementary to the programmable atom equivalents). Reprinted with permission from ref. 123. Copyright 2022 Springer Nature. (d) Tetraivalent caged DNA frameworks and AuNPs formed diamond superlattices. Reprinted with permission from ref. 125. Copyright 2016 The American Association for the Advancement of Science. (e) Complex AuNPs superlattices were formed by hybridization interactions of AuNPs–DNA and the vertex of DNA frames including cube, octahedron, elongated square bipyramid, prism and triangular bipyramid. Reprinted with permission from ref. 124. Copyright 2016 Springer Nature. (f) 3D ordered superlattices of different nanomaterials. Reprinted with permission from ref. 126. Copyright 2020 Springer Nature.

various DNA frames, such as cubes, octahedrons, elongated square bipyramids, prisms, and triangular bipyramids, to form complex AuNP superlattices by hybridization interactions of AuNPs-DNA on the vertex of DNA frames (Fig. 9e).<sup>124</sup> A diamond family of AuNP superlattices was also formed from the tetravalent caged DNA frameworks, which is difficult for DNA-NPs to self-assemble without DNA origami (Fig. 9d).<sup>125</sup> In 2020, they reported a general method for creating 3D ordered superlattices of different nanomaterials using DNA-prescribed and

valence-controlled material voxels (Fig. 9f).<sup>126</sup> Metallic and semiconductor NPs, as well as protein can be encapsulated by DNA frameworks with various valences and assembled into a variety of superlattices.

### 3.5 DNA directed alignment of CNTs

CNTs are among the most desirable carbon materials due to their low density, high tensile strength, and unique thermal, electrical, and optical properties. In addition to individual

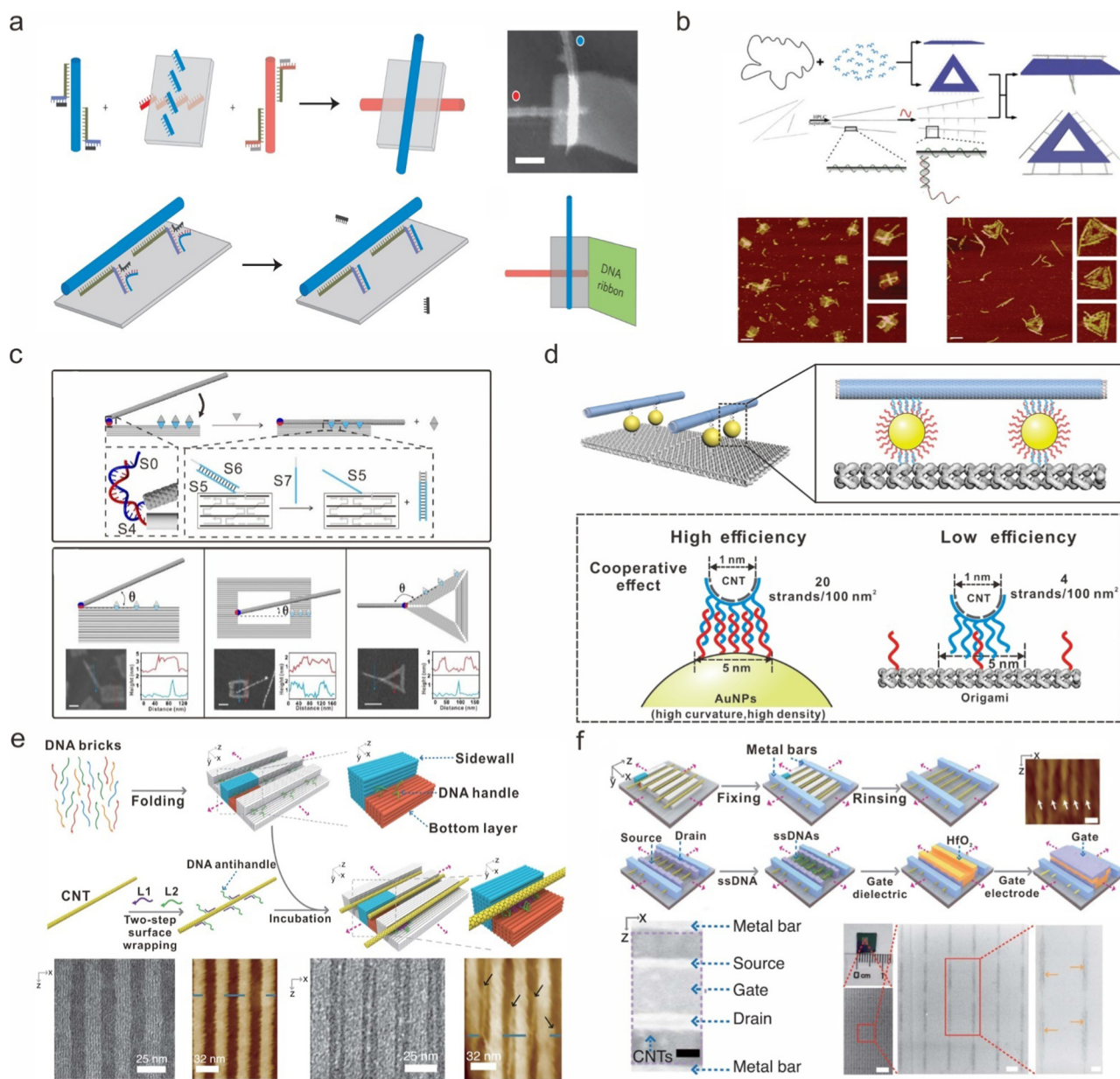


**Fig. 10** DNA directed alignment of CNTs. (a) Assembly of CNTs into cross-junctions by rectangle DNA origami. Reprinted with permission from ref. 127. Copyright 2009 Springer Nature. (b) Assembly of CNTs into complex arrays using triangle and rectangle DNA origami. Reprinted with permission from ref. 128. Copyright 2013 Royal Society of Chemistry. (c) CNTs were placed in precise positions on DNA origami by one-point linkage. Reprinted with permission from ref. 130. Copyright 2019 American Chemical Society. (d) AuNP-mediated highly precise alignment of CNTs on DNA origami. Reprinted with permission from ref. 131. Copyright 2020 John Wiley and Sons. (e) Arrangement of CNTs into parallel arrays templated by DNA SST superstructures. Reprinted with permission from ref. 132. Copyright 2020 The American Association for the Advancement of Science. (f) Application of CNTs arrays in field effect transistor. Reprinted with permission from ref. 133. Copyright 2020 The American Association for the Advancement of Science.

CNTs, ordered arrays of CNTs demonstrated great potential for the development of high-performance electronic devices. Accordingly, a series of CNTs can be aligned sequentially to form ordered arrays using DNA hybridization-directed NP assembly. In 2010, Winfree *et al.* proposed the first DNA origami strategy for arranging CNTs in two dimensions (Fig. 10a).<sup>127</sup> Unlike the simple ssDNA on AuNPs, the DNA strands on CNTs contain a 5 base locked nucleic acid (LNA) toehold, a 15 base protection dsDNA strand, and a 40 base dispersal domain. When mixing DNA origami with DNA-functionalized CNTs, strand displacement mediated the alignment of CNTs into cross-junctions on a DNA origami rectangle. The resulting crossed CNT structure demonstrated a stable field effect transistor (FET) behavior. Yan *et al.* proposed a similar method for aligning discrete CNTs into complex geometries using rectangle and triangle DNA origami (Fig. 10b).<sup>128</sup> In particular, the DNA-wrapped heterogeneous CNTs were sorted using a size exclusion chromatography (SEC) protocol, facilitating the organization of uniform-sized CNTs into superstructures with defined length and inter-tube angles. In addition to the DNA hybridization-based strategy, Norton *et al.* developed an alternative technique to directly align CNTs through strong  $\pi$ - $\pi$  interaction between CNTs and extended ssDNA on DNA origami.<sup>129</sup>

Subsequently, the precision, efficiency, and scale of CNT assembly were further improved. Adrian c. Seeman reported a breakthrough in which CNTs are positioned at precise absolute positions on DNA origami (Fig. 10c).<sup>130</sup> First, DNA end-functionalized CNTs were linked to a specific DNA origami site using a one-point linkage. Several random ssDNA sequences were then extended from DNA origami to immobilize CNTs in parallel or crossed structures through noncovalent interaction. Zuo *et al.* reported an AuNP-mediated technique for highly efficient CNT alignment on DNA origami (Fig. 10d).<sup>131</sup> Due to a higher ssDNA density on spherical nucleic acids (SNAs) than on DNA origami-extended ssDNA, the positioning efficiency of CNTs increased dramatically.

To scale up CNT assembly, Yin *et al.* developed a DNA brick crystal-assisted strategy to align DNA-wrapped CNTs (Fig. 10e).<sup>132</sup> The pitch between CNTs in parallel arrays with more than fifty CNTs can be scaled down to 10.4 nm with an angular deviation of  $<2^\circ$  and an assembly yield of  $>95\%$ . They then constructed bio-templated field-effect transistors (FETs) with parallel CNTs based on these findings (Fig. 10f).<sup>133</sup> Solid-state multichannel CNT FETs demonstrated excellent on-state performance and rapid on-off switching.

## 4 Cell membrane-based approaches for engineering of colloidal NPs

Due to their magnetic, radioactive and plasmonic properties, inorganic NPs play a significant role in fields such as disease diagnosis, imaging and photothermal therapy. Structures of inorganic NPs with small size, low toxicity and high payload are simple to design, functionalize, and assemble, allowing for the incorporation of additional properties and capabilities.<sup>134</sup> *In vitro*, these functions already have significant applications,

but *in vivo*, there are limitations such as precise diagnosis and efficient delivery.<sup>135</sup>

Under physiological conditions, it remains challenging for NPs to achieve effective delivery and diagnosis due to the system's physical and biological barriers, such as shear resistance and protein adsorption.<sup>136,137</sup> These barriers can exist in the system, the environment or the cells, and they are typically heterogeneous and difficult to distinguish and characterize.<sup>138</sup> In addition, the internal environment of the body is extraordinarily complex, allowing it to effectively identify and eliminate external elements. Ultimately, the objective of the desired nanosystem is to engineer NPs with surface stability and biocompatibility that allows them to be ignored except by the target, as well as the realization of immune escape and a long cycle time, which has always been extremely challenging but essential.

Deposition of lipid vesicles (liposomes) on the surface of NPs is a widely used strategy to mimic the cell-like structure,<sup>139</sup> to improve biocompatibility and allow for drug package.<sup>140</sup> Initially, studies focus on the deposition of liposomes at solid interfaces (*e.g.* silica, mica and glass) to form continuous, defect-free and fluid monolayer lipid membranes. On this basis, Brisson *et al.* synthesized liposomes with different charges, including positive, neutral and negative charges.<sup>141</sup> They revealed the formation details of lipid bilayers on silica NPs by cryo-EM, and found that only positively charged and neutral liposomes could form lipid bilayers while negatively charged liposomes did not rupture and flatten. Liu *et al.* reported a general method for preparing lipid-wrapped NPs in aqueous solution.<sup>142</sup> They explored the interaction of ten oxide NPs with liposomes (neutral and anionic charges), and concluded that  $\text{Fe}_3\text{O}_4$  and  $\text{SiO}_2$  formed lipid-encapsulated NPs only with DOCP and DOPC, respectively. However,  $\text{ZnO}$  may cause damage to the phospholipid layer of liposomes.

Recently, various media, such as cell membranes,<sup>143,144</sup> have been developed as coating materials for delivery of NPs with appropriate biocompatibility and cellular or tissue penetration. NPs coated with cell membranes constitute an artificially constructed nanosystem that imitates the surface characteristics of cells to generate new binding properties.<sup>145</sup> The cell membrane is responsible for intercellular communication, immune response and metabolism in the body. Consequently, cell membrane coating can enhance system performance, including biocompatibility, cycle time and penetration. A series of cell types, including red blood cells (RBCs), platelets, white blood cells, cancer cells, stem cells and bacteria, have been used as membrane materials to coat inorganic NPs based on these properties.

Several methods can be used to prepare NPs coated with cell membranes (Fig. 11), the most common being physical extrusion and sonication.<sup>146–148</sup> This method consisted of breaking the membrane structure of donor cells and reconstructing it around the NPs' cores. It is commonly believed that the membrane-coating structure produced by this method has minimal material loss. A microfluidic system is another novel technique for coating NPs with cell membranes.<sup>149</sup> By adjusting

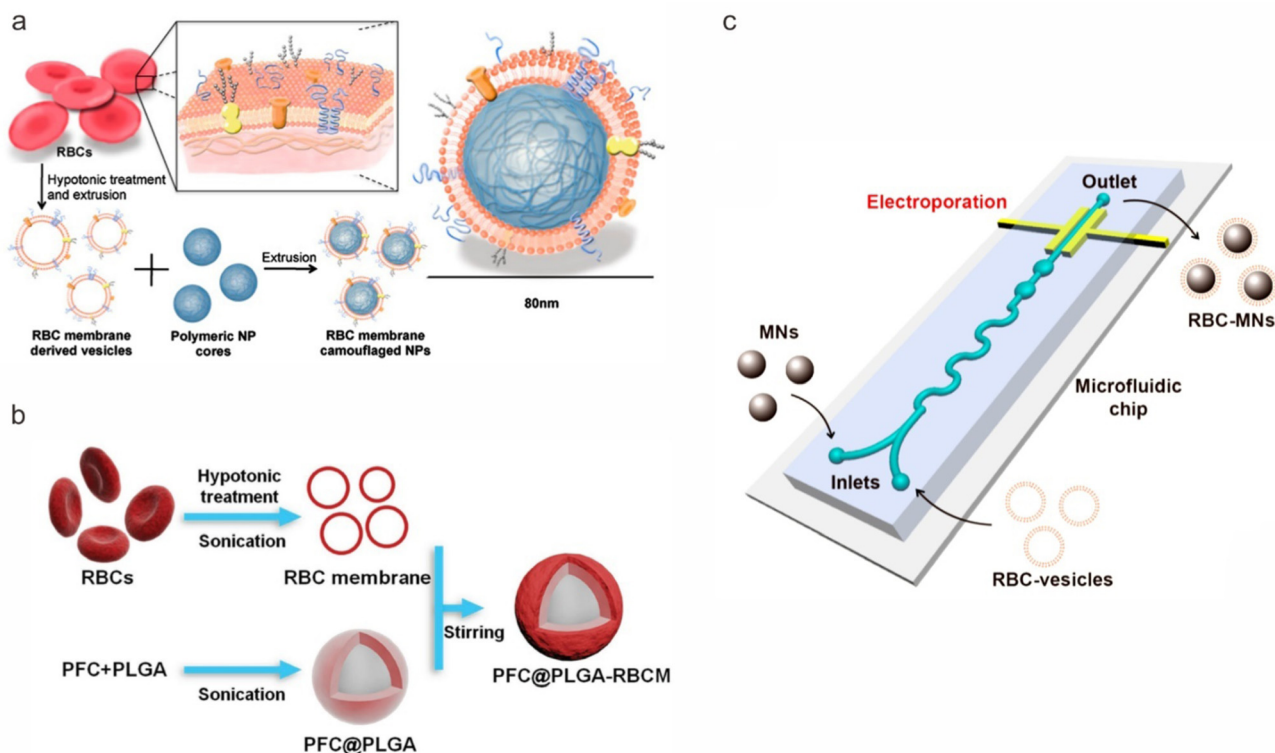


**Fig. 11** Preparation of membrane-coated NPs. (a) Physical extrusion strategy. Reprinted with permission from ref. 146. Copyright 2011 National Academy of Sciences. (b) Ultrasonic strategy. Reprinted with permission from ref. 147. Copyright 2017 John Wiley and Sons. (c) Microfluidic electroporation strategy. Reprinted with permission from ref. 149. Copyright 2017 American Chemical Society.

the pulse voltage, pulse duration, and liquid flow rate, high-quality NP structures with uniform coating and stable performance can be manufactured. Several distinct cell membranes were extracted and used to coat 30–300 nm NPs, thereby enhancing their *in vivo* performance.

#### 4.1 RBC-based approaches

Red blood cells (RBCs) are the most common cells in the body responsible for transporting oxygen. Mature RBCs lack organelles and nuclei, allowing them to pass through blood vessels unharmed and immune system-free. These characteristics are ideal for nanoscale delivery systems and are required for their design. Therefore, RBCs are excellent candidates for encapsulating NPs in order to prevent immune clearance and extend cycle life. In 2011, researchers reported for the first time the RBC membrane coating technology, in which the cell membrane is used directly as an encapsulating material.<sup>146</sup> With a membrane coating on the surface of NPs, the majority of lipids, proteins and carbohydrates can be transferred and preserved, giving membrane-coated NPs many properties same to those of the source cells. In the conventional approach,<sup>150</sup> RBCs were subjected to hypotonic treatment and centrifugation to obtain membrane fragments. Subsequently, ultrasonic sound-waves and extrusion were used to transform the membrane fragments into nanovesicles. By combining NPs and RBC vesicles, the RBC membrane was reconstructed on the surface of NPs, resulting in the formation of NPs coated with RBC membranes

(Fig. 12a). Using this method, a variety of nanoparticles, including gold nanoparticles, mesoporous silica nanoparticles (MSNs), and metal organic frameworks (MOFs), can be coated as the structure's core, allowing for a series of subsequent high-performance diagnostics and treatments. Numerous studies on the synthesis of nanoparticles coated with RBC membranes demonstrate that the coating process has no direct relationship with the size, morphology, and materials of the nanoparticles. Cage-like structures and magnetic cluster structures can also be successfully encapsulated with RBC membranes for imaging and treatment.

#### 4.2 Platelet cell-based approaches

Based on the examples of RBC membrane-coated NPs, platelets have become an important membrane source for relevant exploration and research. Platelets naturally concentrate at injured vessel sites, initiating a series of cascade reactions that result in thrombosis formation in order to maintain hemostasis (Fig. 12b).<sup>151,152</sup> In addition, platelets are associated with a number of other functions and diseases, including cancer, pathogenesis, and infections, which are related to the membrane structure and surface marker expression of platelets. Several disease-relevant functions of platelets can be transferred to NPs by coating them with membranes.

#### 4.3 WBC-based approaches

In a similar manner, white blood cells (WBCs), which are responsible for the execution of immune function, have been

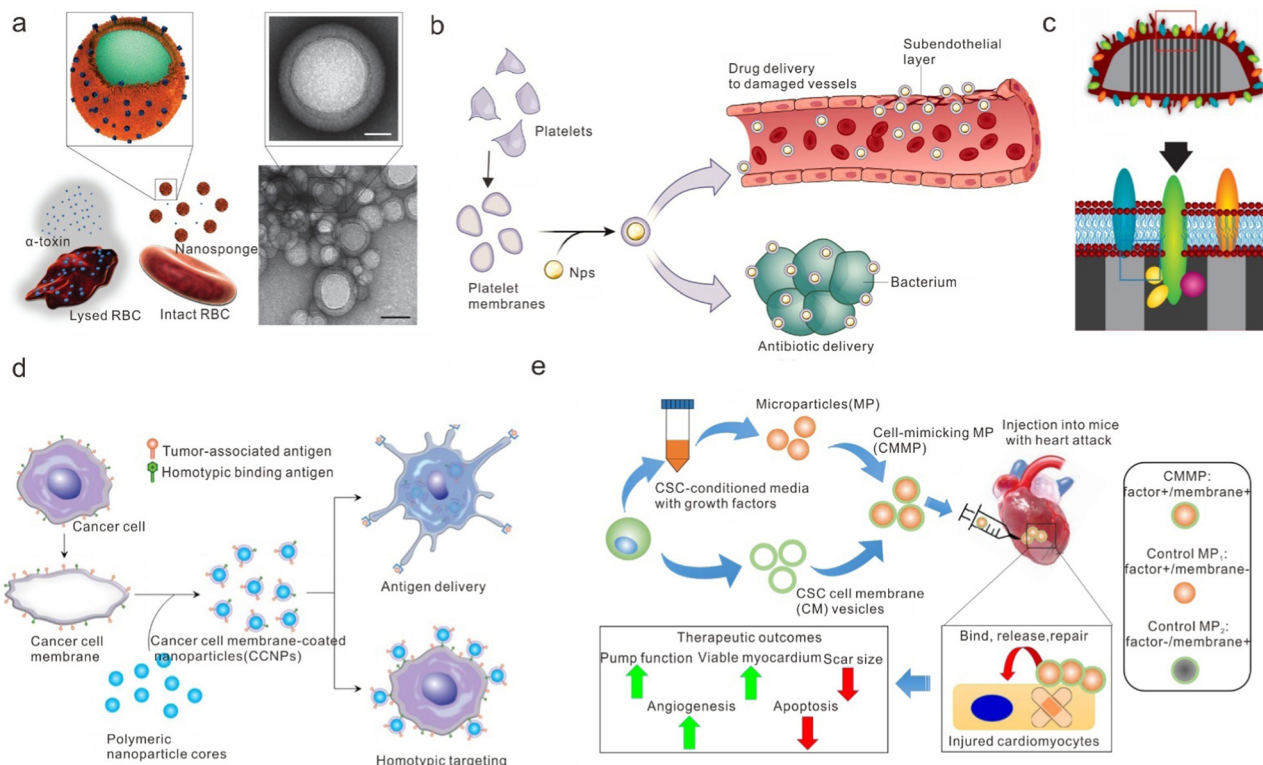


**Fig. 12** Biointerfacing of NPs. (a) NP coating with RBC membranes. Reprinted with permission from ref. 150. Copyright 2013 Springer Nature. (b) NP coating with platelet membranes. Reprinted with permission from ref. 151. Copyright 2015 Springer Nature. (c) NPs coating with WBCs membrane. Reprinted with permission from ref. 144. Copyright 2012 Springer Nature. (d) NP coating with cancer cell membranes. Reprinted with permission from ref. 153. Copyright 2014 American Chemical Society. (e) NP coating with stem cell membranes. Reprinted with permission from ref. 154. Copyright 2017 Springer Nature.

utilized. WBCs include macrophages, B cells, T cells, and neutrophils, among other subsets, compared to RBCs. From a compositional standpoint, white blood cells are nucleated cells with complex internal components and a complicated separation and extraction process. As a result of the excellent specific targeting of WBCs to tumors and vascular disorders (Fig. 12c),<sup>144</sup> new strategies employing NPs incorporated with WBC membranes to create biomimetic nanostructures are advantageous.

#### 4.4 Other approaches

Additionally, numerous other cell types can be utilized to produce membrane coating NPs. Cancer cell membranes possessed the properties of sufficient materials, simple cultivation, and targeting, making them suitable for the construction of membrane-NPs for drug delivery and imaging of cancer (Fig. 12d).<sup>153</sup> Nanoparticles coated with stem cell membranes possessed a unique capacity for tumor tropism and were widely employed in regeneration fields (Fig. 12e).<sup>154</sup> Accordingly, theranostic carriers with high biocompatibility can be constructed using an endothelial cell membrane-based method.<sup>155</sup> The application of NPs coated with beta cell membranes for the treatment of diabetes was of great significance.<sup>156</sup> NPs can be encapsulated in bacterial membrane vesicles in addition to mammalian cell membranes for antibacterial research and vaccine applications.<sup>157,158</sup>

Coating NPs with cell membranes is a promising biomimetic functionalization strategy that integrates the inherent properties of NPs and membranes. On the basis of cell-cell and cell-environment interactions, conventional inorganic NPs generated novel interface functions. Moreover, we can select the type, function, size, charge, and hydrophobicity of NPs and cells to achieve biomedical applications such as drug delivery, imaging and light-activated therapy, toxicity reduction, immune regulation, and detection.

## 5 Applications of surface-engineered colloidal NPs

Recent studies on the interaction between surface-functionalized colloidal NPs and the physiological behavior have revealed a great deal of potential for using these surface-defined nanomaterials for a variety of biomedical applications, including cell type recognition,<sup>159</sup> disease diagnosis,<sup>23</sup> intracellular imaging,<sup>160</sup> and drug/gene delivery.<sup>36</sup> Silica is “generally recognized as safe” (GRAS) by the U.S. Food and Drug Administration (FDA), making it an essential biomaterial for scientific research. Due to their low cytotoxicity, uniform pore size, excellent chemical stability, low cost, versatile functionalization chemistry, and relative ease of large-scale preparation, mesoporous SiO<sub>2</sub> nanoparticles (MSNs) are an ideal material for the

development of novel nanoarchitectures for nanomedicine. In addition, magnetic resonance imaging (MRI) based on MNCs such as  $\text{Fe}_3\text{O}_4$  has evolved into a potent noninvasive imaging tool for assessing tissue function or disease diagnosis with high spatial resolution. Since the discovery of surface-functionalized colloidal NPs, its exceptional properties, such as excellent temporal and spatial resolution, a long effective imaging time window, and fine signal contrast, have attracted the utmost interest of researchers.<sup>161</sup> This section focuses on the cellular uptake and cytotoxicity regulated by the surface properties of colloidal NPs, as well as their imaging, diagnostic, and therapeutic applications.

### 5.1 Cellular uptake of surface-modified colloidal NPs

The cellular uptake of colloidal NPs is significantly influenced by their surface properties. Correspondingly, the ability to manipulate cellular distribution is afforded by the manipulation of these surface properties. PEGylation is a conventional technique in which a hydrating layer is created by attaching PEG to the surface of colloidal NPs. However, PEGylation may not always be the most effective method for developing devices for targeted drug delivery. Wolfgang J. Parak examined the effect of PEG-modified polymer-coated FePt NPs on the adsorption of proteins and the uptake of cultured cells.<sup>25</sup> PEGylated NPs exhibited a marked decrease in cellular uptake, but increased retention times compared to

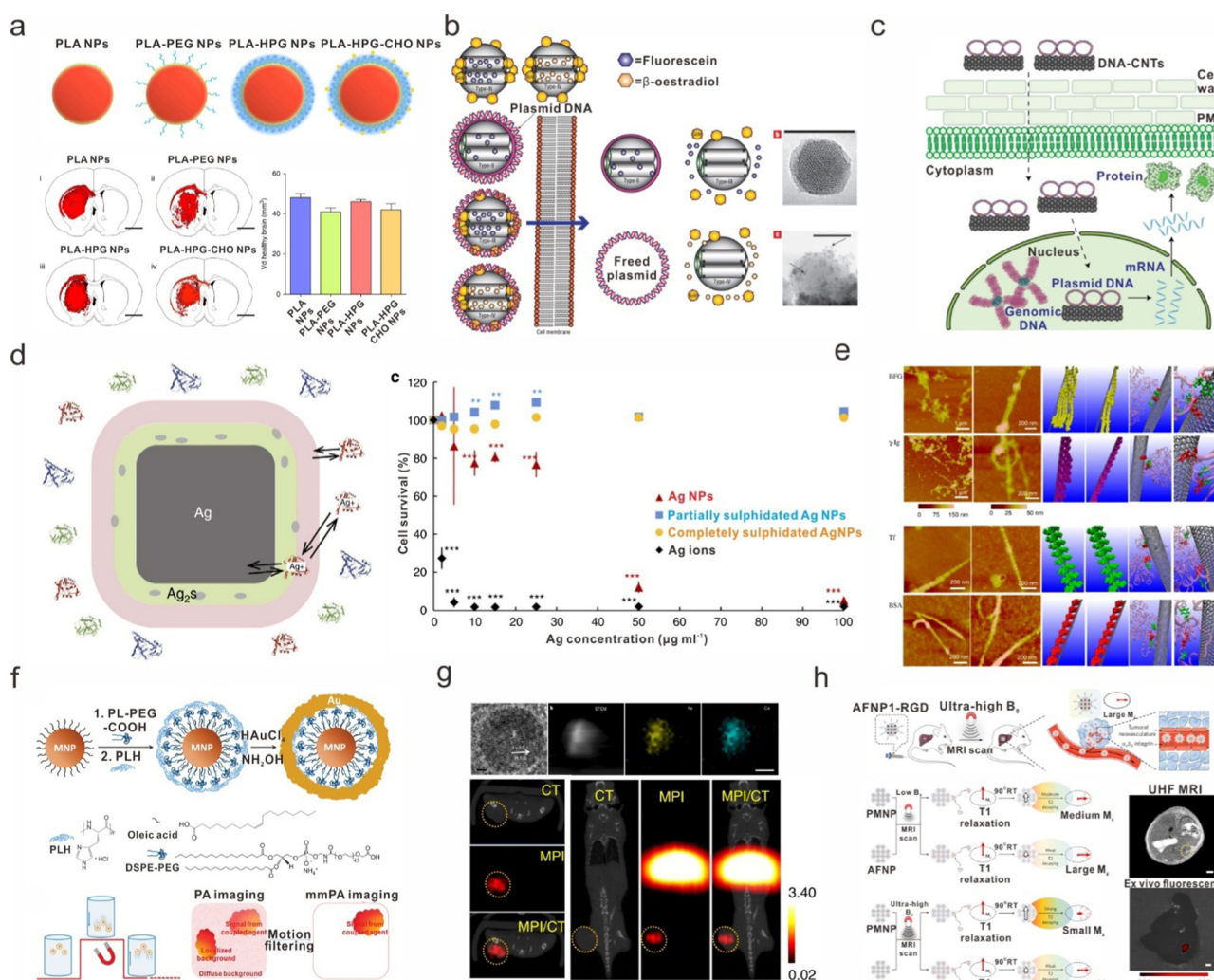


**Fig. 13** Biological behaviors of surface modified colloidal NPs. (a) Effect of PEG modified polymer-FePt NPs on uptake by cells. Reprinted with permission from ref. 162. Copyright 2017 Springer Nature. (b) Gene gun system comprised of AuNPs capped MSNs loaded with DNA genes for plant cell internalization. Reprinted with permission from ref. 166. Copyright 2007 Springer Nature. (c) CNTs-based technologies deliver DNA into plants. Reprinted with permission from ref. 167. Copyright 2019 Springer Nature. (d) Proteins or peptides attached on surface of NPs; a decrease in the toxicity. Reprinted with permission from ref. 168. Copyright 2016 Springer Nature. (e) Protein-coated CNTs changed the cellular interaction pathway, and reduced their cytotoxicity. Reprinted with permission from ref. 64. Copyright 2011 National Academy of Sciences. (f) Multifunctional nanoprobe comprising  $\text{Fe}_3\text{O}_4$  as the core and Au as the shell, showed significantly enhanced contrast for magneto-dynamic photoacoustic imaging. Reprinted with permission from ref. 180. Copyright 2010 Springer Nature. (g) FeCo@C NPs was used as an imaging contrast agent, for magnetic thermotherapy and photothermal ablation. Reprinted with permission from ref. 181. Copyright 2020 Springer Nature. (h) Ultra-sensitive antiferromagnetic NPs probe can target detection of small primary tumors and micrometastases in mice. Reprinted with permission from ref. 182. Copyright 2021 Springer Nature.

unmodified NPs, indicating a paradoxical effect. This phenomenon was also observed when the uptake efficiency of bare-NPs [poly(lactic acid) (PLA)], PEG-NPs, and hyperbranched glycerol aldehydes (HPG-CHO)-NPs was compared (Fig. 13a).<sup>162</sup> The “stealth” properties of PEG-NPs resulted in less internalization than that of bare NPs in brain cells, whereas HPG-CHO-NPs with bioadhesive end-groups demonstrated significantly higher internalization. Due to its ability to extend the circulating lifetimes of nanoparticles *in vivo*, PEG remains the most widely used material.<sup>136,163</sup>

For other surface molecular groups, Lin *et al.* synthesized a series of organically functionalized MSNs and investigated the mechanism and efficiency of endocytosis of various charged MSNs on human cervical cancer cells.<sup>164</sup> Four functional groups, including 3-aminopropyl (AP), guanidinopropyl (GP), 3-[*N*-(2-guanidinoethyl)guanidino]propyl (GEGP), and *N*-folate-3-aminopropyl (FAP), were grafted onto the exterior of FITC-MSNs. They concluded that the endocytosis of MSNs could be manipulated by surface functionalization and using folate groups. The negatively charged MSNs would have a greater buffering capacity, which is essential for endosome escape.

Functional biological materials conjugated to nanoparticles can enhance recognition, cellular uptake, and *in vivo* stability. The carboxyl groups on the surface of MSNs can conjugate with bioactive molecules such as transferrin, as discovered by Prasad *et al.* The cellular uptake of bioconjugated NPs was significantly greater than that of non-bioconjugated NPs.<sup>160</sup> Jose L. Legido fabricated magnetic SiO<sub>2</sub> NPs with DNA fragments affixed to the polyelectrolyte-primed surface.<sup>165</sup> The stoichiometric ratio of positively charged polyelectrolyte to negatively charged DNA determined the zeta-potential and subsequently governed cell-membrane penetration and cytotoxicity.

Surface modification of colloidal NPs can also affect their ability to permeate plant cell walls. Wang *et al.* created a gene gun consisting of AuNP-capped MSNs loaded with DNA genes for plant cell internalization (Fig. 13b).<sup>166</sup> The addition of AuNPs to MSNs increased the complex material's density, allowing it to penetrate plant cell walls and transport DNA into isolated plant cells. Landry *et al.* developed CNT-based technologies that can efficiently and safely deliver DNA into plants in a species-independent manner (Fig. 13c).<sup>167</sup> They utilized DNA-functionalized CNTs as the delivery material, which not only resulted in a high rate of genetic transformation but also protected DNA from nuclease damage.<sup>168</sup>

## 5.2 Cytotoxicity of surface-modified colloidal NPs

Geometry, porosity, and surface characteristics have big influence on the toxicity of colloidal NPs *in vivo*. Ghandehari *et al.* discovered that the *in vivo* toxicity of colloidal NPs was primarily affected by porosity, surface area per mass, and surface charge.<sup>169</sup> When intravenously administered to animals, nonporous SiO<sub>2</sub> NPs exhibited the lowest toxicity with a maximum tolerated dose (MTD) of 450 mg kg<sup>-1</sup>. MSNs with the same geometrical characteristics as nonporous SiO<sub>2</sub> were considerably more toxic. The toxicity of amine-modified MSNs was lower than that of unmodified MSNs, but higher than that of nonporous silica.

They assessed the impact of SiO<sub>2</sub> nanotubes' size and surface charge on their toxicity and uptake by cells.<sup>159</sup> The SiO<sub>2</sub> nanotubes (200 nm) with a larger surface area per mass were significantly more toxic to HUVECs than their longer counterparts (500 nm). However, it was discovered that cell survival statistics complicated the relationship between toxicity and surface charge. At a high SiO<sub>2</sub> concentration (5 microgram per milliliter), the amine-modified SiO<sub>2</sub> NPs were more toxic than the unmodified SiO<sub>2</sub> NPs. At low SiO<sub>2</sub> concentration (0.005 microgram per milliliter), however, the opposite was observed.

To lessen the toxicity of NPs, Christy L. Haynes investigated the hemolytic activity of SiO<sub>2</sub> NPs with and without PEG surface modification.<sup>170</sup> PEG masked the surface silanol groups and prevented additional silanol groups from accessing red blood cells (RBCs), so PEG-modified SiO<sub>2</sub> did not exhibit obvious hemolysis compared to bare SiO<sub>2</sub>. This simple surface modification strategy is indispensable for ensuring the safety of SiO<sub>2</sub> in biomedical applications. Attaching proteins or peptides to the surface of NPs can also reduce toxicity by entrapping NPs within the protein corona, thereby preventing the release of toxic ions into the cell culture media (Fig. 13d).<sup>168</sup> Concerns about the nanotoxicity of these NPs have grown in tandem with the increasing demand for CNTs in biomedicine. Several reports have indicated that CNTs with particular configurations and properties are biotoxic,<sup>171</sup> with long and rigid CNTs having the potential to cause lung damage.<sup>172</sup> Chen *et al.* discovered that protein-coated CNTs alter the cellular interaction pathway and, consequently, diminish their cytotoxicity (Fig. 13e).<sup>64</sup>

## 5.3 Imaging and diagnosis of surface-modified colloidal NPs

Due to their inherent electrical, optical, and magnetic properties, engineered nanoparticles have found widespread application in the nanomedicine field,<sup>173–179</sup> including targeted imaging *in vivo*, early cancer diagnosis, and cancer therapy. Gao *et al.* reported a multifunctional nanoprobe comprising Fe<sub>3</sub>O<sub>4</sub> as the core and Au as the shell (Fig. 13f),<sup>180</sup> which demonstrated significantly improved contrast for magneto-dynamic photoacoustic imaging in comparison to conventional photoacoustic imaging. Rao *et al.* proposed multifunctional FeCo@C NPs that combined the high saturation magnetization of the FeCo core with the strong light absorption of the carbon shell (Fig. 11g).<sup>181</sup> It can be utilized as a contrast agent for MPI, T2 MRI, NIR-II PA, and thermal imaging, as well as to cause rapid heating in magnetic fields for magnetic thermotherapy and photothermal ablation of tumor sites under laser irradiation. Ling *et al.* studied systematically the size, spin alignment patterns, and magnetic moments of various NPs, as well as developed an ultra-sensitive antiferromagnetic NP probe (Fig. 13h).<sup>182</sup> Combining the NP probe and UHF MRI can help detect small primary tumors and micrometastases in mice with a sensitivity and precision comparable to that of histopathological detection.

For non-invasive imaging and therapy, the construction of multifunctional NP complexes capable of achieving rapid, targeted, and highly sensitive identification and eradication of tumors is a significant development trend.<sup>183</sup> However, achieving the early detection of tumors and the diagnosis and

treatment of various biological lesions with high sensitivity at the pathological level remains a challenge.

## 6 Conclusions and perspectives

Surface engineering influences the stability and functions of colloidal NPs, including self-assembly and their physiological behaviors. In this review, we aim to convey the idea that different strategies for surface engineering offer diverse possibilities to achieve controllable and precise NP manipulation in distinct environments. The PEG modification by post-synthesis grafting on SiO<sub>2</sub> NPs using silane-PEG has been proven to be the most widely used strategy to improve the stability in aqueous solutions due to the simplicity of the grafting procedure, the commercial availability of the silane-PEG reagent, and the substantial improvement in stability. However, although PEG can also prevent aggregation in the majority of physiological media, amino groups with long chain alkyl groups by AHAPS surface modification demonstrated greater stability for NPs in media with high ionic concentration. Furthermore, positive surface charge derived from amino groups is necessary for efficient cellular uptake. The size, shape, and surface groups of the synthesized NP complexes can be accurately predicted based on the structure of block copolymer templates for the pre-grafting strategy, which represents a human-designed method for surface engineering of colloidal NPs. Due to the rapid development of DNA-templated nanofabrication, we hypothesized that DNA nanotechnology's high designability in shape and surface properties could increase the complexity of colloidal NPs and their surface properties. The coating of cell membranes can improve system performance, such as biocompatibility, cycle time, and penetration. A series of cell types, including red blood cells (RBCs), platelets, white blood cells, cancer cells, stem cells, and bacteria, have been used as membrane materials to coat inorganic NPs based on these properties.

Despite a series of advances in surface engineering which provide enormous advantages for assembly, detection, imaging and diagnosis, there still remain challenges that need to be addressed. First, the distribution (such as uniformity, density, and solidity) of surface molecules may have different impacts on the stability of NPs. In most of the modification strategies a homogeneous surface was assumed to be formed. However, it is difficult to precisely control the distance, density and number of modified molecules, especially for large polymers at the interface. Moreover, for application in complex biological environments, interfacial molecules may be severely disturbed and blocked by the competing species, therefore affecting the endocytosis, recognition, and translocation effects. This places a higher demand on the reliability of surface engineering. Further optimization of the modification strategies to improve the resistance of NPs in complex matrices is necessary. Finally, further development of oligonucleotide synthesis technology and mechanistic understanding of the NP growth process will greatly expand the scope of future advanced material fabrication and open up new avenues.

## Conflicts of interest

There are no conflicts to declare.

## Acknowledgements

This work was supported by the National Key Research and Development Program of China (no. 2021YFF1200300 and no. 2020YFA0909000), the National Natural Science Foundation of China (no. 22025404, no. 21904086, no. 22104083, and no. 22005187) and the Innovative Research Team of High-Level Local Universities in Shanghai (no. SHSMU-ZLCX20212602).

## References

- Y. Liu, X. Guo, S. Yang, G. He and H. Jin, *Cryst. Res. Technol.*, 2018, **53**, 1700212.
- S.-H. Wu, C.-Y. Mou and H.-P. Lin, *Chem. Soc. Rev.*, 2013, **42**, 3862–3875.
- T. Hyeon, *Chem. Commun.*, 2003, 927–934, DOI: [10.1039/B207789B](https://doi.org/10.1039/B207789B).
- X. Wang, A. Ruditskiy and Y. Xia, *Natl. Sci. Rev.*, 2016, **3**, 520–533.
- M. C. Hersam, *Nat. Nanotechnol.*, 2008, **3**, 387–394.
- C. B. Murray, C. R. Kagan and M. G. Bawendi, *Science*, 1995, **270**, 1335–1338.
- Z. Gao, Y. Hou, J. Zeng, L. Chen, C. Liu, W. Yang and M. Gao, *Adv. Mater.*, 2017, **29**, 1701095.
- S. C. Tsang, V. Caps, I. Paraskevas, D. Chadwick and D. Thompsett, *Angew. Chem., Int. Ed.*, 2004, **43**, 5645–5649.
- W. Li, J. Liu and D. Zhao, *Nat. Rev. Mater.*, 2016, **1**, 16023.
- B. Wang, X. Wang, J. Zou, Y. Yan, S. Xie, G. Hu, Y. Li and A. Dong, *Nano Lett.*, 2017, **17**, 2003–2009.
- N. Liu and T. Liedl, *Chem. Rev.*, 2018, **118**, 3032–3053.
- E. T. Thostenson, Z. Ren and T.-W. Chou, *Compos. Sci. Technol.*, 2001, **61**, 1899–1912.
- M. P. Anantram and F. Léonard, *Rep. Prog. Phys.*, 2006, **69**, 507.
- P. Avouris, Z. Chen and V. Perebeinos, *Nat. Nanotechnol.*, 2007, **2**, 605–615.
- J.-C. Charlier, X. Blase and S. Roche, *Rev. Mod. Phys.*, 2007, **79**, 677–732.
- B. K. Kaushik, S. Goel and G. Rauthan, *Microelectron. Int.*, 2007, **24**, 53–63.
- B. Mahar, C. Laslau, R. Yip and Y. Sun, *IEEE Sens. J.*, 2007, **7**, 266–284.
- C. Graf, Q. Gao, I. Schütz, C. N. Noufele, W. Ruan, U. Posselt, E. Korotianskiy, D. Nordmeyer, F. Rancan, S. Hadam, A. Vogt, J. Lademann, V. Haucke and E. Rühl, *Langmuir*, 2012, **28**, 7598–7613.
- Q.-G. Wang, L. He, L.-Y. Zhao, R.-S. Liu, W.-P. Zhang and A.-H. Lu, *Adv. Funct. Mater.*, 2020, **30**, 1906117.
- K.-C. Park, H. J. Choi, C.-H. Chang, R. E. Cohen, G. H. McKinley and G. Barbastathis, *ACS Nano*, 2012, **6**, 3789–3799.

- 21 T. A. Meyer, C. Zhang, G. Bao and Y. Ke, *Nano Lett.*, 2020, **20**, 2799–2805.
- 22 F. Caruso, *Adv. Mater.*, 2001, **13**, 11–22.
- 23 D. Shi, H. S. Cho, Y. Chen, H. Xu, H. Gu, J. Lian, W. Wang, G. Liu, C. Huth, L. Wang, R. C. Ewing, S. Budko, G. M. Pauletti and Z. Dong, *Adv. Mater.*, 2009, **21**, 2170–2173.
- 24 M. B. Gawande, P. S. Branco and R. S. Varma, *Chem. Soc. Rev.*, 2013, **42**, 3371–3393.
- 25 B. Pelaz, P. del Pino, P. Maffre, R. Hartmann, M. Gallego, S. Rivera-Fernández, J. M. de la Fuente, G. U. Nienhaus and W. J. Parak, *ACS Nano*, 2015, **9**, 6996–7008.
- 26 J. Gregory, *J. Colloid Interface Sci.*, 1981, **83**, 138–145.
- 27 M. A. Butkus and D. Grasso, *J. Colloid Interface Sci.*, 1998, **200**, 172–181.
- 28 Y.-S. Lin, N. Abadeer, K. R. Hurley and C. L. Haynes, *J. Am. Chem. Soc.*, 2011, **133**, 20444–20457.
- 29 R. Hogg, T. W. Healy and D. W. Fuerstenau, *Trans. Faraday Soc.*, 1966, **62**, 1638–1651.
- 30 S. Edwards and D. Williams, *Phys. Rev. Lett.*, 2004, **92**, 248303.
- 31 B. Derjaguin, *Kolloid-Z.*, 1934, **69**, 155–164.
- 32 L. Qiao, Z. Fu, J. Li, J. Ghosen, M. Zeng, J. Stebbins, P. N. Prasad and M. T. Swihart, *ACS Nano*, 2017, **11**, 6370–6381.
- 33 W. Li, J. Yang, Z. Wu, J. Wang, B. Li, S. Feng, Y. Deng, F. Zhang and D. Zhao, *J. Am. Chem. Soc.*, 2012, **134**, 11864–11867.
- 34 D. Dollimore, Silica chemistry, *Nature*, 1980, **283**, 510.
- 35 L. H. Reddy, J. L. Arias, J. Nicolas and P. Couvreur, *Chem. Rev.*, 2012, **112**, 5818–5878.
- 36 M. Wu, Q. Meng, Y. Chen, L. Zhang, M. Li, X. Cai, Y. Li, P. Yu, L. Zhang and J. Shi, *Adv. Mater.*, 2016, **28**, 1963–1969.
- 37 K. Ma, Y. Gong, T. Aubert, M. Z. Turker, T. Kao, P. C. Doerschuk and U. Wiesner, *Nature*, 2018, **558**, 577–580.
- 38 K. Bridger and B. Vincent, *Eur. Polym. J.*, 1980, **16**, 1017–1021.
- 39 T.-J. Yoon, J. S. Kim, B. G. Kim, K. N. Yu, M.-H. Cho and J.-K. Lee, *Angew. Chem., Int. Ed.*, 2005, **44**, 1068–1071.
- 40 K. Ma, D. Zhang, Y. Cong and U. Wiesner, *Chem. Mater.*, 2016, **28**, 1537–1545.
- 41 V. Cauda, C. Argyo and T. Bein, *J. Mater. Chem.*, 2010, **20**, 8693–8699.
- 42 R. P. Bagwe, L. R. Hilliard and W. Tan, *Langmuir*, 2006, **22**, 4357–4362.
- 43 M. Stefkik, S. Guldin, S. Vignolini, U. Wiesner and U. Steiner, *Chem. Soc. Rev.*, 2015, **44**, 5076–5091.
- 44 X. Pang, L. Zhao, W. Han, X. Xin and Z. Lin, *Nat. Nanotechnol.*, 2013, **8**, 426–431.
- 45 H. Xu, F. Yan, E. E. Monson and R. Kopelman, *J. Biomed. Mater. Res., Part A*, 2003, **66A**, 870–879.
- 46 S. Sun, H. Zeng, D. B. Robinson, S. Raoux, P. M. Rice, S. X. Wang and G. Li, *J. Am. Chem. Soc.*, 2004, **126**, 273–279.
- 47 T. Fried, G. Shemer and G. Markovich, *Adv. Mater.*, 2001, **13**, 1158–1161.
- 48 H. Deng, X. Li, Q. Peng, X. Wang, J. Chen and Y. Li, *Angew. Chem., Int. Ed.*, 2005, **44**, 2782–2785.
- 49 R. Janot and D. Guérard, *J. Alloys Compd.*, 2002, **333**, 302–307.
- 50 J. Muro-Cruces, A. G. Roca, A. López-Ortega, E. Fantechi, D. del-Pozo-Bueno, S. Estradé, F. Peiró, B. Sepúlveda, F. Pineider, C. Sangregorio and J. Nogues, *ACS Nano*, 2019, **13**, 7716–7728.
- 51 Y. Liu, T. Chen, C. Wu, L. Qiu, R. Hu, J. Li, S. Cansiz, L. Zhang, C. Cui, G. Zhu, M. You, T. Zhang and W. Tan, *J. Am. Chem. Soc.*, 2014, **136**, 12552–12555.
- 52 Y. Liu, D. L. Purich, C. Wu, Y. Wu, T. Chen, C. Cui, L. Zhang, S. Cansiz, W. Hou, Y. Wang, S. Yang and W. Tan, *J. Am. Chem. Soc.*, 2015, **137**, 14952–14958.
- 53 Y. Wang, J. F. Wong, X. Teng, X. Z. Lin and H. Yang, *Nano Lett.*, 2003, **3**, 1555–1559.
- 54 T. Zhang, J. Ge, Y. Hu and Y. Yin, *Nano Lett.*, 2007, **7**, 3203–3207.
- 55 H. Wu, H. Zhu, J. Zhuang, S. Yang, C. Liu and Y. C. Cao, *Angew. Chem., Int. Ed.*, 2008, **47**, 3730–3734.
- 56 A. Prakash, H. Zhu, C. J. Jones, D. N. Benoit, A. Z. Ellsworth, E. L. Bryant and V. L. Colvin, *ACS Nano*, 2009, **3**, 2139–2146.
- 57 Y.-M. Huh, Y.-w Jun, H.-T. Song, S. Kim, J.-s Choi, J.-H. Lee, S. Yoon, K.-S. Kim, J.-S. Shin, J.-S. Suh and J. Cheon, *J. Am. Chem. Soc.*, 2005, **127**, 12387–12391.
- 58 J.-H. Lee, Y.-w Jun, S.-I. Yeon, J.-S. Shin and J. Cheon, *Angew. Chem., Int. Ed.*, 2006, **45**, 8160–8162.
- 59 A. Dong, X. Ye, J. Chen, Y. Kang, T. Gordon, J. M. Kikkawa and C. B. Murray, *J. Am. Chem. Soc.*, 2011, **133**, 998–1006.
- 60 Y. Yuan, Z. Ding, J. Qian, J. Zhang, J. Xu, X. Dong, T. Han, S. Ge, Y. Luo, Y. Wang, K. Zhong and G. Liang, *Nano Lett.*, 2016, **16**, 2686–2691.
- 61 E. T. Mickelson, C. B. Huffman, A. G. Rinzler, R. E. Smalley, R. H. Hauge and J. L. Margrave, *Chem. Phys. Lett.*, 1998, **296**, 188–194.
- 62 M. X. Pulikkathara, O. V. Kuznetsov and V. N. Khabashesku, *Chem. Mater.*, 2008, **20**, 2685–2695.
- 63 W. H. Duan, Q. Wang and F. Collins, *Chem. Sci.*, 2011, **2**, 1407–1413.
- 64 C. Ge, J. Du, L. Zhao, L. Wang, Y. Liu, D. Li, Y. Yang, R. Zhou, Y. Zhao, Z. Chai and C. Chen, *Proc. Natl. Acad. Sci. U. S. A.*, 2011, **108**, 16968–16973.
- 65 V. Zorbas, A. Ortiz-Acevedo, A. B. Dalton, M. M. Yoshida, G. R. Dieckmann, R. K. Draper, R. H. Baughman, M. Jose-Yacaman and I. H. Musselman, *J. Am. Chem. Soc.*, 2004, **126**, 7222–7227.
- 66 A. Ortiz-Acevedo, H. Xie, V. Zorbas, W. M. Sampson, A. B. Dalton, R. H. Baughman, R. K. Draper, I. H. Musselman and G. R. Dieckmann, *J. Am. Chem. Soc.*, 2005, **127**, 9512–9517.
- 67 M. Saint-Cricq, J. Carrete, C. Gaboriaud, E. Gravel, E. Doris, N. Thielens, N. Mingo and W. L. Ling, *Nano Lett.*, 2017, **17**, 3409–3415.
- 68 B. K. Price and J. M. Tour, *J. Am. Chem. Soc.*, 2006, **128**, 12899–12904.
- 69 C. Wang, B. Meany and Y. Wang, *Angew. Chem., Int. Ed.*, 2017, **56**, 9326–9330.

- 70 A. Nish, J.-Y. Hwang, J. Doig and R. J. Nicholas, *Nat. Nanotechnol.*, 2007, **2**, 640–646.
- 71 M. Zheng, A. Jagota, E. D. Semke, B. A. Diner, R. S. McLean, S. R. Lustig, R. E. Richardson and N. G. Tassi, *Nat. Mater.*, 2003, **2**, 338–342.
- 72 M. Zheng, A. Jagota, M. S. Strano, A. P. Santos, P. Barone, S. G. Chou, B. A. Diner, M. S. Dresselhaus, R. S. McLean, G. B. Onoa, G. G. Samsonidze, E. D. Semke, M. Usrey and D. J. Walls, *Science*, 2003, **302**, 1545–1548.
- 73 X. Tu, S. Manohar, A. Jagota and M. Zheng, *Nature*, 2009, **460**, 250–253.
- 74 G. Ao, J. K. Streit, J. A. Fagan and M. Zheng, *J. Am. Chem. Soc.*, 2016, **138**, 16677–16685.
- 75 Y. Zhang, F. Li, M. Li, X. Mao, X. Jing, X. Liu, Q. Li, J. Li, L. Wang, C. Fan and X. Zuo, *J. Am. Chem. Soc.*, 2019, **141**, 17861–17866.
- 76 Y. Min, M. Akbulut, K. Kristiansen, Y. Golan and J. Israelachvili, *Nat. Mater.*, 2008, **7**, 527–538.
- 77 M. A. Boles, M. Engel and D. V. Talapin, *Chem. Rev.*, 2016, **116**, 11220–11289.
- 78 F. Hong, F. Zhang, Y. Liu and H. Yan, *Chem. Rev.*, 2017, **117**, 12584–12640.
- 79 K. A. Dill and J. L. MacCallum, *Science*, 2012, **338**, 1042–1046.
- 80 I. A. Chen and P. Walde, *Cold Spring Harbor Perspect. Biol.*, 2010, **2**, a002170.
- 81 F. S. Bates, M. A. Hillmyer, T. P. Lodge, C. M. Bates, K. T. Delaney and G. H. Fredrickson, *Science*, 2012, **336**, 434–440.
- 82 S. Sun, C. B. Murray, D. Weller, L. Folks and A. Moser, *Science*, 2000, **287**, 1989–1992.
- 83 E. V. Shevchenko and D. V. Talapin, in *Semiconductor Nanocrystal Quantum Dots: Synthesis, Assembly, Spectroscopy and Applications*, ed. A. L. Rogach, Springer, Vienna, 2008, pp. 119–169.
- 84 T. P. Bigioni, X.-M. Lin, T. T. Nguyen, E. I. Corwin, T. A. Witten and H. M. Jaeger, *Nat. Mater.*, 2006, **5**, 265–270.
- 85 A. Dong, J. Chen, P. M. Vora, J. M. Kikkawa and C. B. Murray, *Nature*, 2010, **466**, 474–477.
- 86 M. R. Jones, N. C. Seeman and C. A. Mirkin, *Science*, 2015, **347**, 1260901.
- 87 W. B. Rogers, W. M. Shih and V. N. Manoharan, *Nat. Rev. Mater.*, 2016, **1**, 16008.
- 88 G. Yao, F. Zhang, F. Wang, T. Peng, H. Liu, E. Poppleton, P. Šulc, S. Jiang, L. Liu, C. Gong, X. Jing, X. Liu, L. Wang, Y. Liu, C. Fan and H. Yan, *Nat. Chem.*, 2020, **12**, 1067–1075.
- 89 P. Song, J. Shen, D. Ye, B. Dong, F. Wang, H. Pei, J. Wang, J. Shi, L. Wang, W. Xue, Y. Huang, G. Huang, X. Zuo and C. Fan, *Nat. Commun.*, 2020, **11**, 838.
- 90 M. Li, H. Ding, M. Lin, F. Yin, L. Song, X. Mao, F. Li, Z. Ge, L. Wang, X. Zuo, Y. Ma and C. Fan, *J. Am. Chem. Soc.*, 2019, **141**, 18910–18915.
- 91 M. Lin, P. Song, G. Zhou, X. Zuo, A. Aldalbahi, X. Lou, J. Shi and C. Fan, *Nat. Commun.*, 2016, **11**, 1244–1263.
- 92 Z. Li, Q. Fan and Y. Yin, *Chem. Rev.*, 2022, **122**, 4976–5067.
- 93 J. I. Cutler, E. Auyeung and C. A. Mirkin, *J. Am. Chem. Soc.*, 2012, **134**, 1376–1391.
- 94 J. J. Storhoff, R. Elghanian, R. C. Mucic, C. A. Mirkin and R. L. Letsinger, *J. Am. Chem. Soc.*, 1998, **120**, 1959–1964.
- 95 X. Zhang, M. R. Servos and J. Liu, *J. Am. Chem. Soc.*, 2012, **134**, 7266–7269.
- 96 B. Liu and J. Liu, *J. Am. Chem. Soc.*, 2017, **139**, 9471–9474.
- 97 B. Liu, T. Wu, Z. Huang, Y. Liu and J. Liu, *Angew. Chem., Int. Ed.*, 2019, **58**, 2109–2113.
- 98 Y. Hao, Y. Li, L. Song and Z. Deng, *J. Am. Chem. Soc.*, 2021, **143**, 3065–3069.
- 99 M. Huang, E. Xiong, Y. Wang, M. Hu, H. Yue, T. Tian, D. Zhu, H. Liu and X. Zhou, *Nat. Commun.*, 2022, **13**, 968.
- 100 Y. Wang, Y. Wang, X. Zheng, É. Ducrot, M.-G. Lee, G.-R. Yi, M. Weck and D. J. Pine, *J. Am. Chem. Soc.*, 2015, **137**, 10760–10766.
- 101 T. G. W. Edwardson, K. L. Lau, D. Bousmail, C. J. Serpell and H. F. Sleiman, *Nat. Chem.*, 2016, **8**, 162–170.
- 102 G. Yao, J. Li, Q. Li, X. Chen, X. Liu, F. Wang, Z. Qu, Z. Ge, R. P. Narayanan, D. Williams, H. Pei, X. Zuo, L. Wang, H. Yan, B. L. Feringa and C. Fan, *Nat. Mater.*, 2020, **19**, 781–788.
- 103 G. Chen, K. J. Gibson, D. Liu, H. C. Rees, J.-H. Lee, W. Xia, R. Lin, H. L. Xin, O. Gang and Y. Weizmann, *Nat. Mater.*, 2019, **18**, 169–174.
- 104 G. Paniagua, A. Villalonga, M. Eguílaz, B. Vegas, C. Parrado, G. Rivas, P. Díez and R. Villalonga, *Anal. Chim. Acta*, 2019, **1061**, 84–91.
- 105 R. Kadam, J. Ghawali, M. Waespy, M. Maas and K. Rezwan, *Nanoscale*, 2020, **12**, 18938–18949.
- 106 X. Zhang, Y. Ge, M. Liu, Y. Pei, P. He, W. Song and S. Zhang, *Anal. Chem.*, 2022, **94**, 7823–7832.
- 107 Y. Gao and Y. Yu, *J. Am. Chem. Soc.*, 2013, **135**, 19091–19094.
- 108 H. Xing, Z. Wang, Z. Xu, N. Y. Wong, Y. Xiang, G. L. Liu and Y. Lu, *ACS Nano*, 2012, **6**, 802–809.
- 109 G. Zhu, Z. Xu, Y. Yang, X. Dai and L.-T. Yan, *ACS Nano*, 2018, **12**, 9467–9475.
- 110 P. W. K. Rothemund, *Nature*, 2006, **440**, 297–302.
- 111 B. Wei, M. Dai and P. Yin, *Nature*, 2012, **485**, 623–626.
- 112 J. Zheng, J. J. Birktoft, Y. Chen, T. Wang, R. Sha, P. E. Constantinou, S. L. Ginell, C. Mao and N. C. Seeman, *Nature*, 2009, **461**, 74–77.
- 113 A. Kuzyk, R. Schreiber, Z. Fan, G. Pardatscher, E.-M. Roller, A. Högele, F. C. Simmel, A. O. Govorov and T. Liedl, *Nature*, 2012, **483**, 311–314.
- 114 X. Lan, X. Lu, C. Shen, Y. Ke, W. Ni and Q. Wang, *J. Am. Chem. Soc.*, 2015, **137**, 457–462.
- 115 P. Zhan, T. Wen, Z.-G. Wang, Y. He, J. Shi, T. Wang, X. Liu, G. Lu and B. Ding, *Angew. Chem., Int. Ed.*, 2018, **57**, 2846–2850.
- 116 R. Schreiber, J. Do, E.-M. Roller, T. Zhang, V. J. Schüller, P. C. Nickels, J. Feldmann and T. Liedl, *Nat. Nanotechnol.*, 2014, **9**, 74–78.
- 117 T. Zhang, A. Neumann, J. Lindlau, Y. Wu, G. Pramanik, B. Naydenov, F. Jelezko, F. Schüder, S. Huber, M. Huber,

- F. Stehr, A. Högele, T. Weil and T. Liedl, *J. Am. Chem. Soc.*, 2015, **137**, 9776–9779.
- 118 D. Nykypanchuk, M. M. Maye, D. van der Lelie and O. Gang, *Nature*, 2008, **451**, 549–552.
- 119 S. Y. Park, A. K. R. Lytton-Jean, B. Lee, S. Weigand, G. C. Schatz and C. A. Mirkin, *Nature*, 2008, **451**, 553–556.
- 120 R. J. Macfarlane, B. Lee, M. R. Jones, N. Harris, G. C. Schatz and C. A. Mirkin, *Science*, 2011, **334**, 204–208.
- 121 C. R. Laramy, M. N. O'Brien and C. A. Mirkin, *Nat. Rev. Mater.*, 2019, **4**, 201–224.
- 122 M. N. O'Brien, M. R. Jones, B. Lee and C. A. Mirkin, *Nat. Mater.*, 2015, **14**, 833–839.
- 123 S. Wang, S. Lee, J. S. Du, B. E. Partridge, H. F. Cheng, W. Zhou, V. P. Dravid, B. Lee, S. C. Glotzer and C. A. Mirkin, *Nat. Mater.*, 2022, **21**, 580–587.
- 124 Y. Tian, Y. Zhang, T. Wang, H. L. Xin, H. Li and O. Gang, *Nat. Mater.*, 2016, **15**, 654–661.
- 125 W. Liu, M. Tagawa, H. L. Xin, T. Wang, H. Emamy, H. Li, K. G. Yager, F. W. Starr, A. V. Tkachenko and O. Gang, *Science*, 2016, **351**, 582–586.
- 126 Y. Tian, J. R. Lhermitte, L. Bai, T. Vo, H. L. Xin, H. Li, R. Li, M. Fukuto, K. G. Yager, J. S. Kahn, Y. Xiong, B. Minevich, S. K. Kumar and O. Gang, *Nat. Mater.*, 2020, **19**, 789–796.
- 127 H. T. Maune, S.-p Han, R. D. Barish, M. Bockrath, W. A. G. Iii, P. W. K. Rothemund and E. Winfree, *Nat. Nanotechnol.*, 2010, **5**, 61–66.
- 128 Z. Zhao, Y. Liu and H. Yan, *Org. Biomol. Chem.*, 2013, **11**, 596–598.
- 129 A. Mangalum, M. Rahman and M. L. Norton, *J. Am. Chem. Soc.*, 2013, **135**, 2451–2454.
- 130 H. Pei, R. Sha, X. Wang, M. Zheng, C. Fan, J. W. Canary and N. C. Seeman, *J. Am. Chem. Soc.*, 2019, **141**, 11923–11928.
- 131 Y. Zhang, X. Mao, F. Li, M. Li, X. Jing, Z. Ge, L. Wang, K. Liu, H. Zhang, C. Fan and X. Zuo, *Angew. Chem., Int. Ed.*, 2020, **59**, 4892–4896.
- 132 W. Sun, J. Shen, Z. Zhao, N. Arellano, C. Rettner, J. Tang, T. Cao, Z. Zhou, T. Ta, J. K. Streit, J. A. Fagan, T. Schaus, M. Zheng, S.-J. Han, W. M. Shih, H. T. Maune and P. Yin, *Science*, 2020, **368**, 874–877.
- 133 M. Zhao, Y. Chen, K. Wang, Z. Zhang, J. K. Streit, J. A. Fagan, J. Tang, M. Zheng, C. Yang, Z. Zhu and W. Sun, *Science*, 2020, **368**, 878–881.
- 134 C. Xu, J. Nam, H. Hong, Y. Xu and J. J. Moon, *ACS Nano*, 2019, **13**, 12148–12161.
- 135 K.-W. Huang, F.-F. Hsu, J. T. Qiu, G.-J. Chern, Y.-A. Lee, C.-C. Chang, Y.-T. Huang, Y.-C. Sung, C.-C. Chiang, R.-L. Huang, C.-C. Lin, T. K. Dinh, H.-C. Huang, Y.-C. Shih, D. Alson, C.-Y. Lin, Y.-C. Lin, P.-C. Chang, S.-Y. Lin and Y. Chen, *Sci. Adv.*, 2020, **6**, eaax5032.
- 136 E. Blanco, H. Shen and M. Ferrari, *Nat. Biotechnol.*, 2015, **33**, 941–951.
- 137 S. N. Bhatia, X. Chen, M. A. Dobrovolskaia and T. Lammers, *Nat. Rev. Cancer*, 2022, **22**, 550–556.
- 138 S. Wilhelm, A. J. Tavares, Q. Dai, S. Ohta, J. Audet, H. F. Dvorak and W. C. W. Chan, *Nat. Rev. Mater.*, 2016, **1**, 16014.
- 139 J. Liu, *Langmuir*, 2016, **32**, 4393–4404.
- 140 B. Wang, L. Zhang, S. C. Bae and S. Granick, *Proc. Natl. Acad. Sci. U. S. A.*, 2008, **105**, 18171–18175.
- 141 S. Mornet, O. Lambert, E. Duguet and A. Brisson, *Nano Lett.*, 2005, **5**, 281–285.
- 142 F. Wang, X. Zhang, Y. Liu, Z. Y. Lin, B. Liu and J. Liu, *Angew. Chem., Int. Ed.*, 2016, **55**, 12063–12067.
- 143 M. T. Stephan and D. J. Irvine, *Nano Today*, 2011, **6**, 309–325.
- 144 A. Parodi, N. Quattrocihi, A. L. van de Ven, C. Chiappini, M. Evangelopoulos, J. O. Martinez, B. S. Brown, S. Z. Khaled, I. K. Yazdi, M. V. Enzo, L. Isenhart, M. Ferrari and E. Tasciotti, *Nat. Nanotechnol.*, 2013, **8**, 61–68.
- 145 R. H. Fang, A. V. Kroll, W. Gao and L. Zhang, *Adv. Mater.*, 2018, **30**, 1706759.
- 146 C.-M. J. Hu, L. Zhang, S. Aryal, C. Cheung, R. H. Fang and L. Zhang, *Proc. Natl. Acad. Sci. U. S. A.*, 2011, **108**, 10980–10985.
- 147 M. Gao, C. Liang, X. Song, Q. Chen, Q. Jin, C. Wang and Z. Liu, *Adv. Mater.*, 2017, **29**, 1701429.
- 148 J. A. Copp, R. H. Fang, B. T. Luk, C.-M. J. Hu, W. Gao, K. Zhang and L. Zhang, *Proc. Natl. Acad. Sci. U. S. A.*, 2014, **111**, 13481–13486.
- 149 L. Rao, B. Cai, L.-L. Bu, Q.-Q. Liao, S.-S. Guo, X.-Z. Zhao, W.-F. Dong and W. Liu, *ACS Nano*, 2017, **11**, 3496–3505.
- 150 C.-M. J. Hu, R. H. Fang, J. Copp, B. T. Luk and L. Zhang, *Nat. Nanotechnol.*, 2013, **8**, 336–340.
- 151 O. C. Farokhzad, *Nature*, 2015, **526**, 47–48.
- 152 C.-M. J. Hu, R. H. Fang, K.-C. Wang, B. T. Luk, S. Thamphiwatana, D. Dehaini, P. Nguyen, P. Angsantikul, C. H. Wen, A. V. Kroll, C. Carpenter, M. Ramesh, V. Qu, S. H. Patel, J. Zhu, W. Shi, F. M. Hofman, T. C. Chen, W. Gao, K. Zhang, S. Chien and L. Zhang, *Nature*, 2015, **526**, 118–121.
- 153 R. H. Fang, C.-M. J. Hu, B. T. Luk, W. Gao, J. A. Copp, Y. Tai, D. E. O'Connor and L. Zhang, *Nano Lett.*, 2014, **14**, 2181–2188.
- 154 J. Tang, D. Shen, T. G. Caranasos, Z. Wang, A. C. Vandergriff, T. A. Allen, M. T. Hensley, P.-U. Dinh, J. Cores, T.-S. Li, J. Zhang, Q. Kan and K. Cheng, *Nat. Commun.*, 2017, **8**, 13724.
- 155 A. K. Andriola Silva, R. Di Corato, T. Pellegrino, S. Chat, G. Pugliese, N. Luciani, F. Gazeau and C. Wilhelm, *Nanoscale*, 2013, **5**, 11374–11384.
- 156 W. Chen, Q. Zhang, B. T. Luk, R. H. Fang, Y. Liu, W. Gao and L. Zhang, *Nanoscale*, 2016, **8**, 10364–10370.
- 157 W. Gao, R. H. Fang, S. Thamphiwatana, B. T. Luk, J. Li, P. Angsantikul, Q. Zhang, C.-M. J. Hu and L. Zhang, *Nano Lett.*, 2015, **15**, 1403–1409.
- 158 J. Shao, M. Xuan, H. Zhang, X. Lin, Z. Wu and Q. He, *Angew. Chem., Int. Ed.*, 2017, **56**, 12935–12939.
- 159 A. Nan, X. Bai, S. J. Son, S. B. Lee and H. Ghandehari, *Nano Lett.*, 2008, **8**, 2150–2154.
- 160 R. Kumar, I. Roy, T. Y. Ohulchanskyy, L. N. Goswami, A. C. Bonoiu, E. J. Bergey, K. M. Tramposch, A. Maitra and P. N. Prasad, *ACS Nano*, 2008, **2**, 449–456.

- 161 M. G. Shapiro, R. M. Ramirez, L. J. Sperling, G. Sun, J. Sun, A. Pines, D. V. Schaffer and V. S. Bajaj, *Nat. Chem.*, 2014, **6**, 629–634.
- 162 E. Song, A. Gaudin, A. R. King, Y.-E. Seo, H.-W. Suh, Y. Deng, J. Cui, G. T. Tietjen, A. Huttner and W. M. Saltzman, *Nat. Commun.*, 2017, **8**, 15322.
- 163 J. A. Finbloom, F. Sousa, M. M. Stevens and T. A. Desai, *Adv. Drug Delivery Rev.*, 2020, **167**, 89–108.
- 164 I. Slowing, B. G. Trewyn and V. S. Y. Lin, *J. Am. Chem. Soc.*, 2006, **128**, 14792–14793.
- 165 A. B. Davila-Ibanez, V. Salgueirino, V. Martinez-Zorzano, R. Mariño-Fernández, A. García-Lorenzo, M. Maceira-Campos, M. Muñoz-Ubeda, E. Junquera, E. Aicart, J. Rivas, F. J. Rodriguez-Berrocal and J. L. Legido, *ACS Nano*, 2012, **6**, 747–759.
- 166 F. Torney, B. G. Trewyn, V. S. Y. Lin and K. Wang, *Nat. Nanotechnol.*, 2007, **2**, 295–300.
- 167 G. S. Demirer, H. Zhang, J. L. Matos, N. S. Goh, F. J. Cunningham, Y. Sung, R. Chang, A. J. Aditham, L. Chio, M.-J. Cho, B. Staskawicz and M. P. Landry, *Nat. Nanotechnol.*, 2019, **14**, 456–464.
- 168 T. Miclăuș, C. Beer, J. Chevallier, C. Scavenius, V. E. Bochenkov, J. J. Enghild and D. S. Sutherland, *Nat. Commun.*, 2016, **7**, 11770.
- 169 T. Yu, K. Greish, L. D. McGill, A. Ray and H. Ghandehari, *ACS Nano*, 2012, **6**, 2289–2301.
- 170 Y.-S. Lin and C. L. Haynes, *J. Am. Chem. Soc.*, 2010, **132**, 4834–4842.
- 171 X. Lu, Y. Zhu, R. Bai, Z. Wu, W. Qian, L. Yang, R. Cai, H. Yan, T. Li, V. Pandey, Y. Liu, P. E. Lobie, C. Chen and T. Zhu, *Nat. Nanotechnol.*, 2019, **14**, 719–727.
- 172 M. Gravely, A. Kindopp, L. Hubert, M. Card, A. Nadeem, C. Miller and D. Roxbury, *ACS Appl. Mater. Interfaces*, 2022, **14**, 19168–19177.
- 173 P. Cheng and K. Pu, *Nat. Rev. Mater.*, 2021, **6**, 1095–1113.
- 174 W. Chen, M. Schilperoort, Y. Cao, J. Shi, I. Tabas and W. Tao, *Nat. Rev. Cardiol.*, 2022, **19**, 228–249.
- 175 B. Du, M. Yu and J. Zheng, *Nat. Rev. Mater.*, 2018, **3**, 358–374.
- 176 S. Liu, X. Chen, L. Bao, T. Liu, P. Yuan, X. Yang, X. Qiu, J. J. Gooding, Y. Bai, J. Xiao, F. Pu and Y. Jin, *Nat. Biomed. Eng.*, 2020, **4**, 1063–1075.
- 177 S. Sindhwani, A. M. Syed, J. Ngai, B. R. Kingston, L. Maiorino, J. Rothschild, P. MacMillan, Y. Zhang, N. U. Rajesh, T. Hoang, J. L. Y. Wu, S. Wilhelm, A. Zilman, S. Gadde, A. Sulaiman, B. Ouyang, Z. Lin, L. Wang, M. Egeblad and W. C. W. Chan, *Nat. Mater.*, 2020, **19**, 566–575.
- 178 L. Fan, W. Wang, Z. Wang and M. Zhao, *Nat. Commun.*, 2021, **12**, 6371.
- 179 J. W. Myerson, P. N. Patel, K. M. Rubey, M. E. Zamora, M. H. Zaleski, N. Habibi, L. R. Walsh, Y.-W. Lee, D. C. Luther, L. T. Ferguson, O. A. Marcos-Contreras, P. M. Glassman, L. L. Mazaleuskaya, I. Johnston, E. D. Hood, T. Shuvaeva, J. Wu, H.-Y. Zhang, J. V. Gregory, R. Y. Kiseleva, J. Nong, T. Grosser, C. F. Greineder, S. Mitragotri, G. S. Worthen, V. M. Rotello, J. Lahann, V. R. Muzykantov and J. S. Brenner, *Nat. Nanotechnol.*, 2022, **17**, 86–97.
- 180 Y. Jin, C. Jia, S.-W. Huang, M. O'Donnell and X. Gao, *Nat. Commun.*, 2010, **1**, 41.
- 181 G. Song, M. Kenney, Y.-S. Chen, X. Zheng, Y. Deng, Z. Chen, S. X. Wang, S. S. Gambhir, H. Dai and J. Rao, *Nat. Biomed. Eng.*, 2020, **4**, 325–334.
- 182 Z. Liang, Q. Wang, H. Liao, M. Zhao, J. Lee, C. Yang, F. Li and D. Ling, *Nat. Commun.*, 2021, **12**, 3840.
- 183 F. Yin, M. Li, X. Mao, F. Li, X. Xiang, Q. Li, L. Wang, X. Zuo, C. Fan and Y. Zhu, *Angew. Chem., Int. Ed.*, 2020, **59**, 10406.